Shear wave velocity estimation in the Bengal Basin, Bangladesh by HVSR analysis: implications for engineering bedrock depth

AUTHOR(S):

Farazi, Atikul Haque; Hossain, Md. Shakhawat; Ito, Yoshihiro; Piña-Flores, José; Kamal, A.S.M. Maksud; Rahman, Md. Zillur

CITATION:

Farazi, Atikul Haque ...[et al]. Shear wave velocity estimation in the Bengal Basin, Bangladesh by HVSR analysis: implications for engineering bedrock depth. Journal of Applied Geophysics 2023, 211: 104967.

ISSUE DATE:

2023-04

URL:

http://hdl.handle.net/2433/284055

Journal of Applied Geophysics 211 (2023) 104967

Contents lists available at ScienceDirect

Journal of Applied Geophysics

journal homepage: www.elsevier.com/locate/jappgeo

Shear wave velocity estimation in the Bengal Basin, Bangladesh by HVSR analysis: implications for engineering bedrock depth

Atikul Haque Farazi [a,b], Md. Shakhawat Hossain [c,*], Yoshihiro Ito [d], José Piña-Flores [e], A.S.M. Maksud Kamal [c], Md. Zillur Rahman [c]

[a] Division of Earth and Planetary Sciences, Kyoto University, Kyoto 611-0011, Japan
[b] Department of Geology and Mining, University of Barishal, Barishal 8200, Bangladesh
[c] Department of Disaster Science and Climate Resilience, University of Dhaka, Dhaka 1000, Bangladesh
[d] Disaster Prevention Research Institute, Kyoto University, Kyoto 611-0011, Japan
[e] Facultad de Ingeniería, Universidad Nacional Autónoma de México, Ciudad de México, Mexico

ARTICLE INFO

Keywords:
HVSR
S-wave velocity
Engineering bedrock
Seismic site response
Seismic hazard
Bengal Basin

ABSTRACT

The S-wave velocity (V_S) in the Bengal Basin, Bangladesh has not been resolved from the ground surface to an intermediate depth in a regional context despite its importance for seismic hazard and risk evaluation. For this reason, we estimated V_S profiles beneath 19 seismic stations in Bangladesh to a depth approximately 2800 m by employing full horizontal to vertical spectral ratio (HVSR) curve inversion under the diffuse field theory for the noise wavefield. The seismic stations are concentrated in three tectonic zones within the basin: the Surma basin (SB, Zone 1), Bengal Foredeep (BF, Zone 2), and Chittagong Tripura Fold Belt (CTFB, Zone 3). Full HVSR analysis (from 0.2 to 10 Hz) allowed us to obtain deep profiles with combined insights from shallow geotechnical boreholes and deep P-wave velocity (V_P) information from active seismic surveys. From the resultant V_S profiles, engineering bedrock ($V_S > 760$ m/s) depths were also identified throughout the study area for the first time. The V_S profiles within the Holocene to Miocene sedimentary sequences showed rapid variations from location to location. This is due to the highly variable near-surface geology caused by the dense and complex river network and tectonic deformation in Bangladesh. Except for three stations, the engineering bedrock depth exceeded 30 m at all stations. These results indicate the existence of deep soft soil in the study area, where V_S^{30} based site characterization is inappropriate. Furthermore, seismic site response was estimated at a station (DHAK) by simulating a subduction zone earthquake. The resulting response spectrum (RS) exhibited ground motion amplification over a longer period, suggesting that multistory buildings at the site may be at risk if subjected to large earthquakes. The outcomes of this study can serve as useful guidelines for seismic risk reduction planning in Bangladesh.

1. Introduction

The Bengal Basin in Bangladesh (Fig. 1) is one of the most densely populated areas in the world, hosting over 160 million people (Bürgi et al., 2021). Being on the northeast (NE) toe of the Indian Craton, this country is bisected by the boundary between the Indian and Burmese plates, which on average, has a north-south (N-S) alignment (Bilham, 2004; Mahmud et al., 2020).

Bangladesh is adjacent to active subduction zones along the Indo-Eurasian (between the Indian and Eurasian plates) and blind Indo-Burmese (between the Indian and Eurasian plates) plate boundaries to the North and in the East, respectively (Steckler et al., 2008). Moreover, the Dauki fault, the source of the great Assam earthquake of 1897 (Oldham, 1899), is located along the northernmost part of the country. Several large, destructive earthquakes have occurred along plate boundaries and faults in India and Bangladesh (Bilham, 2004). Several earthquakes of magnitude ≥3 have also occurred in and around this country in the recent past (Rahman et al., 2018). A list of historic earthquakes and their effects in Bangladesh is available in the Banglapedia (https://en.banglapedia.org/index.php/Earthquake). Earthquake

Abbreviations: HVSR, Horizontal-to-vertical spectral ratio.

* Corresponding author.
E-mail address: shakhawat.dsm@du.ac.bd (Md.S. Hossain).

https://doi.org/10.1016/j.jappgeo.2023.104967
Received 16 April 2022; Received in revised form 24 January 2023; Accepted 7 February 2023
Available online 10 February 2023

records indicate that the country is vulnerable to seismic activity (Steckler et al., 2008). The fact that destructive earthquakes may occur near Bangladesh has also been ascertained in recent studies using Global Positioning System (GPS) measurements (Steckler et al., 2016) and reflection profiles with sonic logs (Bürgi et al., 2021). Moreover, in the foothills of the Himalayan Mountains, this downstream riverine region is filled with soft sediments. Soft sedimentary layers over engineering bedrock (S-wave velocity, V_S, > 760 m/s), which we will frequently term as "bedrock" hereinafter, can potentially amplify earthquake ground motion. Bedrock depth also significantly controls the phenomena of soil-infrastructure vibration and resonance when subjected to the ground motion of an earthquake (Manea et al., 2020; Rahman et al., 2021).

Therefore, for seismic risk mitigation through hazard estimation and subsequent planning, it is important to have adequate information on soft sediment thickness or sediment-bedrock interface depth. Seismic site characterization, however, is generally performed based on the average V_S of the upper 30 m of the subsurface, commonly known as "V_S^{30} analysis" (Bajaj and Anbazhagan, 2019). Such analysis is appropriate in areas with shallow (< 30 m) bedrock but could be misleading in areas with thick (> 30 m) soft sediments (Rahman et al., 2021). Rahman et al. (2021) estimated bedrock depth at ten scattered sites in the Dhaka City and found bedrock at a depth of >175 m. Therefore, they concluded that V_S^{30} based seismic site characterization is not suitable at these sites. It is not surprising that engineering bedrock depth exceeds 30 m in a deep sedimentary basin. Therefore, determination of bedrock depth throughout the country is extremely important for developing seismic risk reduction planning in this region. In this context, we have made the first effort to estimate engineering bedrock from the surface to an intermediate depth regionally in the Bengal Basin, Bangladesh utilizing data from the available seismic stations (Fig. 1). The study was accomplished by analyzing the full horizontal-to-vertical spectral ratio (HVSR) of the ambient noise.

Ambient seismic noise (ASN) is produced by natural phenomena, *e.g.*, oceanic waves and winds (termed "microseisms" and commonly below 1 Hz), or by human activities, *e.g.*, industries and traffics (termed "microtremors" and commonly above 1 Hz) (Bonnefoy-Claudet et al., 2006; Farazi et al., 2023). ASN-based methods have been applied effectively in the past decades for imaging both shallow and deep structures because of their efficiency, ease of deployment, and low cost, whereas direct drilling and active source seismic methods are expensive, time consuming, and infeasible for deployment in urban areas. These imaging techniques can be divided into seismic array and single-station methods. The extraction of the surface wave dispersion by applying the spatial auto-correlation technique (SPAC; Aki, 1957), frequency-

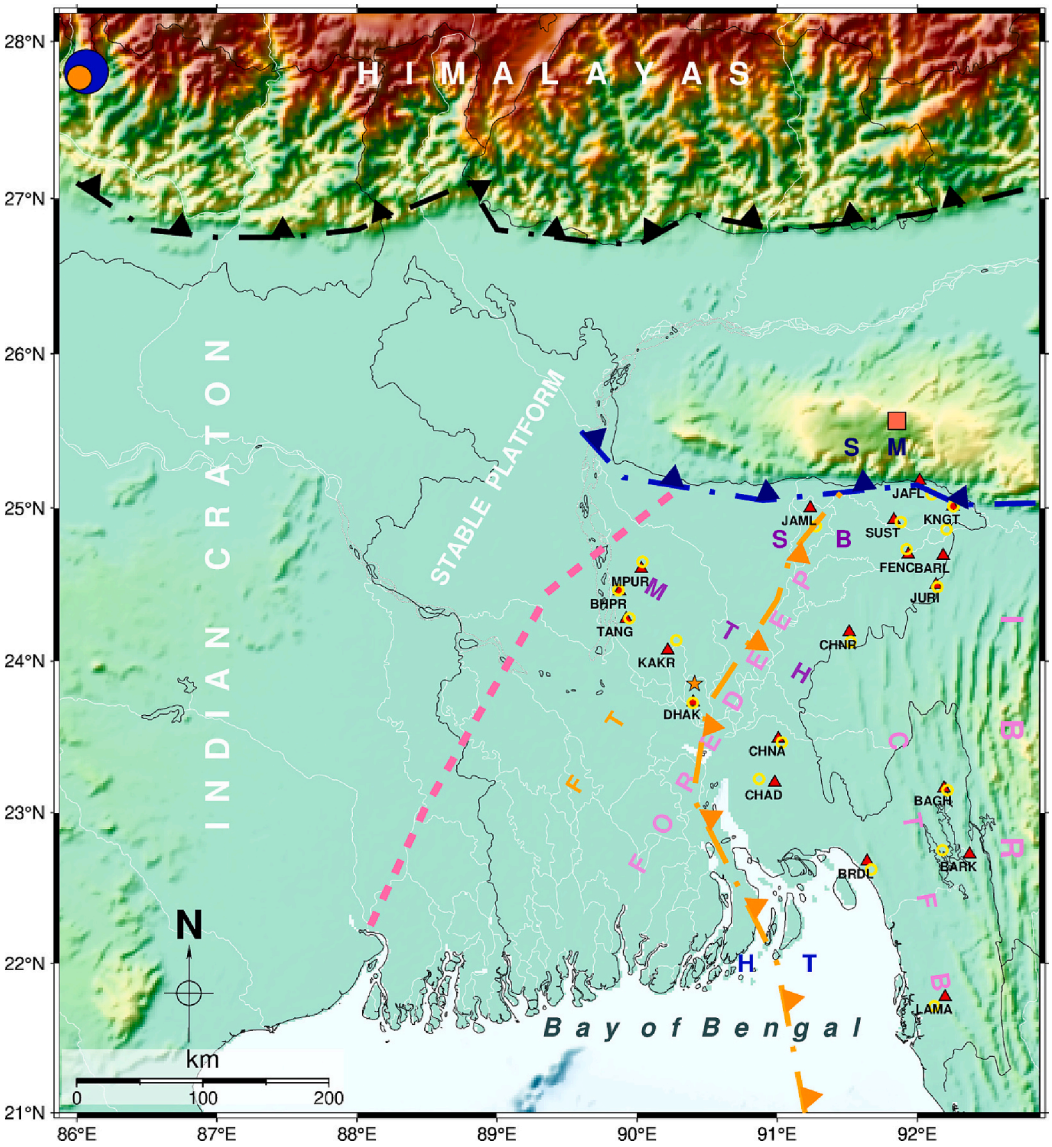

Fig. 1. Map showing tectonic elements of the Bengal Basin along with distribution of the seismic stations of this study. Blue dashed dotted line indicates the Dauki fault. Orange dashed dotted line indicates the inferred Indo-Burmese plate boundary thrust. Black dashed line manifests the Indo-Eurasian plate boundary thrust. Triangle direction with these lines indicates subduction direction. Pink dashed line indicates the Eocene Hinge Zone. The red triangles indicate the seismic stations with the station code given by the text below. The open yellow circles demonstrate the Bangladesh Water development Board (BWDB) borehole positions. The red square symbolizes station SHL for the site response study. The blue and orange circles indicate the locations of the M_W 7.3 and 6.7 earthquakes, respectively (Table 5). The orange colour star denotes Dhaka, the capital city of Bangladesh. CTFB: Chittagong Tripura fold belt; FT: Faridpur trough; HT: Hatiya Trough; MTH: Madhupur Tripura High; SB: Surma basin; SM: Shilling Massif. The tectonic elements are from Alam et al. (2003) and Steckler et al. (2016). (For interpretation of the references to colour in this figure legend, the reader is referred to the web version of this article.)

wavenumber technique (*f*-k; Lacoss et al., 1969), interferometric multichannel analysis of surface waves (IMASW; Lontsi et al., 2016), wavefield decomposition technique (WaveDec, Maranò et al., 2012), and other relevant methods along with the subsequent inversion for underground V_S profiles exemplify the seismic array techniques. Surface wave tomography can also be performed by the cross-correlation of ASN array records (Shapiro et al., 2005). In addition, the subsurface V_S profile can be obtained by inverting the single-station HVSR curve.

The HVSR technique relies on the impedance contrast of subsurface layers, resulting in a frequency response (Bonnefoy-Claudet et al., 2006; Piña-Flores et al., 2017). The H/V spectrum is extremely sensitive to vertical changes in impedance contrast, whereas the tomographic methods are efficient in detecting lateral contrast in the subsurface (Perton et al., 2020). In this study, we used the ASN-based single-station HVSR method to obtain the V_S profile below a seismic station.

For simplicity of analysis, ease of data collection, and cost efficiency, the passive and non-invasive single-station HVSR method has been widely utilized in the past decades for site response studies (Nakamura, 1989) and underground V_S profile estimation (Arai and Tokimatsu, 2004). In addition, this technique can be applied anywhere, even where there is no seismicity, because the omnipresent natural vibration of the earth is sufficient for such a deployment (Perton et al., 2020). Several recent studies have demonstrated the utilization of the HVSR method in retrieving deep crustal structures at depths of several thousand meters (Perton et al., 2020; Farazi et al., 2023), in contrast to its conventional application for shallow (~200 m, Nakamura, 1989) or intermediate depths (~2000 m, Asten et al., 2014).

The HVSR method is efficient in providing on-site information, but the physics behind HVSR curve inversion and forward modelling for obtaining subsurface V_S structures is dubious (Molnar et al., 2018, 2022). Nakamura (1989, 2000) interpreted the HVSR curve using the V_S transfer function, while others argued that the curve is predominantly composed of surface waves (Arai and Tokimatsu, 2004), and still others related it to Rayleigh wave ellipticity (Fäh et al., 2003). Recently, based on the diffuse field assumption (DFA) of the ASN wavefield, Sánchez-Sesma et al. (2011) proposed that the HVSR of noise comprises of all types of waves, that is, body and surface waves. They associated the HVSR of Nakamura (1989) with the directional energy density (DED) and the imaginary parts of the Green's functions (GF) of the horizontal and vertical components. Such a DFA-based interpretation has facilitated the full HVSR curve inversion for subsurface velocity profiles (for example, Lontsi et al., 2015; García-Jerez et al., 2016; Wu et al., 2017). Herein, we adopted the forward modelling and inversion software HV-Inv (García-Jerez et al., 2016), which uses DFA theory for HVSR analysis.

A total of 19 seismic stations in the Bengal Basin (Fig. 1) were used in this study to obtain V_S profiles down to intermediate depths (maximum of ~2800 m). To our knowledge, HVSR inversion, considering DFA theory, has not yet been applied in this region for retrieving subsurface V_S profiles. Subsurface V_S information is crucial for exploration purposes, site response analysis, seismic site characterization and microzonation, seismic tomographic studies, and the detection of fast and slow earthquakes in this region.

Additionally, as an example of what can be expected from a large earthquake in this region, a site response analysis was performed at site DHAK (in the capital city of Dhaka, Bangladesh). For this purpose, the response spectrum (RS) was computed by simulating a subduction zone earthquake using several hundred meters of soil column information obtained from HVSR curve inversion of this study. RS aids in projecting the forces that the structures at a site would experience during an earthquake. Thus, a similar seismic hazard analysis for rest of the sites of this study, and various earthquakes will be invoked for future work, which may be useful for estimating the seismic risk in Bangladesh.

2. Study area

2.1. Tectonic setting

The Bengal Basin (Fig. 1), a pericratonic foreland basin in the northeastern toe of the Indian Craton, is one of the largest sedimentary basins worldwide and that is occupied primarily by Bangladesh and parts of eastern India. The major tectonic features bounding the basin are the exposed Indian Craton (or the Indian Plate) to the west, Shillong Massif to the north, Indo-Burmese Ranges (IBR) to the east, and Bay of Bengal to the south.

The northward collision and convergence of the Indian Plate with the Eurasian Plate during the Eocene gave rise to the Himalayan Ranges (during the Oligocene to Miocene); subsequently, the Bengal Basin was created along the eastern toe of the Indian Plate (Molnar and Tapponnier, 1975; Davies et al., 2003). Later, between the Eocene and Oligocene, the Burmese Plate began overriding the Indian Plate from the east, following an oblique collision (Davies et al., 2003; Steckler et al., 2008). As a result, the Himalayan Arc of the Indo-Eurasian plate boundary and the Burma Arc of the Indo-Burmese plate boundary override the Indian Plate from the north and the east, respectively (Ni et al., 1989). Thus, the Assam Basin is formed between the Indian Plate and Himalayan Arc, whereas the Bengal Basin is formed between the Indian Plate and the Burma Arc as foreland basins of the Indian Plate. Consequently, the Bengal Basin lies at the junction of the Indian, Eurasian, and Burmese plates (Alam et al., 2003).

The Himalayan Ranges have been the major source of sediments for the basin since the Cretaceous (Alam et al., 2003). The paleo-Ganges River from the west and paleo-Brahmaputra River from the east primarily supplied sediments in the Bengal Basin (Davies et al., 2003) to form one of the world's thickest (± 20 km) sedimentary basins, which is composed of early Cretaceous to Holocene sedimentary successions (Alam et al., 2003). Then the Meghna River started draining part of the Surma basin from the NE, as well as part of the Chittagong Tripura fold belt (CTFB) and IBR from the east. It subsequently joined the Ganges and Brahmaputra Rivers downstream of their confluence to form the Ganges-Brahmaputra-Meghna (GBM) delta, also popularly known as the "Bengal Delta".

The basin can be subdivided into three broad tectonic provinces: (1) the stable shelf in the west, (2) the deep basin zone, and (3) the CTFB (Fig. 1, Alam et al., 2003). The first two tectonic provinces are demarcated by the hinge zone (Fig. 1, Steckler et al., 2016). The thickness of the sedimentary successions in the first province varies from ~200–6000 m, while it is ~3000–25,000 m in the other provinces (Alam et al., 2003; Singh et al., 2016).

In this study, we concentrated on the deeper basin portion (Provinces 2 and 3) of the Bengal basin because the seismic stations of this study are available only across these structural provinces (Fig. 1). Following the seismic station distribution and tectonic setting, we compartmentalized the current study area into three zones from north to south: (1) Zone 1, within the Surma basin (SB); (2) Zone 2, within the Bengal foredeep (BF) area, which includes the Madhupur-Comilla tract (MCT); and (3) Zone 3, within the CTFB (Fig. 1).

The BF (Zone 2) in the central part of the deep basin consists of poorly connected sub-basins: the SB (also known as the "Sylhet Trough"), Faridpur Trough, and Hatia Trough from north to south (Khan and Chouhan, 1996). The active basin, as a result of the ongoing orogenesis of the two adjacent arc systems, has experienced intrabasinal faulting to form the sub-basins (Goodbred et al., 2003). Another consequence of faulting is the upliftment of the Madhupur Tract during the Pleistocene and the Comilla Tract during the Holocene (Goodbred et al., 2003). However, the MCT clearly separates the SB from the Faridpur Trough.

Thick deposits of the Bengal Basin suffered significant uplift in two areas: (1) along the northern and the eastern margins of the SB in NE Bangladesh and (2) the CTFB in eastern Bangladesh (Uddin and

Lundberg, 1999). The swampy SB (Zone 1) is a flexural depocenter in the northeastern Bangladesh, with the thickest (~25 km) sedimentary successions (Bürgi et al., 2021). The active Dauki Fault is the northern limit of the SB as well as the Bengal Basin, along which the Shillong Massif (Fig. 1) rose from the Late Miocene (Johnson and Alam, 1991). Overthrusting of the Shillong Plateau, as a forward jump of the Himalayan fault, causes continuous subsidence in its foreland SB (Alam et al., 2003).

The CTFB (Zone 3) has a conspicuously different landscape due to the N-S trending anticlines, which resulted from the westward continuation of the IBR, resting on the décollement megathrust of the arc-trench system of the Indian Plate and Burma Arc. This zone is a consequence of ongoing deformation along the subduction zone (Khan and Chouhan, 1996). The elevation from the west is close to the sea level but rises to ~1500 m within the IBR (Bürgi et al., 2021).

2.2. Stratigraphy

The deep basin consists of Cretaceous–Holocene sediments (Alam et al., 2003). However, in the study area, the stratigraphy of the shallow to intermediate depths is dominated by Miocene to Holocene sedimentary successions. Several hundred meters of the basin are filled by less compacted Holocene deposits, loose sand dominating fluvial Dihing Formation, and loose sand dominating fluvial Dupi Tila Formation. The general Miocene to Holocene stratigraphy of Zones 1, 2, and 3 is described in Tables 1, 2, and 3, respectively. However, local stratigraphy is subject to frequent facies changes due to variations in river morphology (Small et al., 2009). Stratigraphic information of sedimentary deposits is significant because of the lithological composition and compaction, which typically increase with age, potentially controlling the engineering properties of the subsurface geological material.

2.3. Physiography

The GBM River system has established a very dense and complex network of tributaries and distributaries in the Bengal Basin (Alam et al., 2003). The river system and neotectonic activities (Goodbred and Kuehl, 2000) have sculptured the physiography of the Bengal Basin, which can be subdivided into three prominent units: (1) Holocene floodplains, (2) Pleistocene terraces, and (3) Tertiary hills (Goodbred and Kuehl, 2000). The latter two units were severely dissected by the rivers. The physiography of Bangladesh could be further subdivided into 24-subregions and 54 units (Physiography-Banglapedia, https://en.banglapedia.org/index.php/Physiography). Physiographic units often have control over the engineering properties of the geological materials within the shallow subsurface. The physiographic units of Bangladesh are illustrated in Fig. 2, in which it is evident that the three zones of this study have distinct physiographies.

3. Data processing

As part of the global effort to evaluate the geohazard risk of the tectonically active Ganges-Brahmaputra Delta, arrays of seismic stations were deployed in the Bengal Basin. Among the arrays, XI (https://doi.org/10.7914/SN/XI_2007), Z6 (https://doi.org/10.7914/SN/Z6_2011), and BI (https://www.fdsn.org/networks/detail/BI/) are publicly available on the Incorporated Research Institutes for Seismology (IRIS) website. From the 21 stations, this study used 19 stations owing to the data quality of the remaining two (MANK and SKPR), and the four-character codes corresponding to the stations are shown in Fig. 1. However, this study used continuous records for 15 days from each station. As a reference hard site, for site response analysis, we chose Shillong, Meghalaya, India (Sadiq et al., 2018) and used data from station SHL (Fig. 1), operated by the Indian Meteorological Department, India (https://www.fdsn.org/networks/detail/IN/). The summarized information on the network, location, and instrumentation is provided in Supplementary Table 1. Before further analysis, instrumental response removal, mean and trend removal, tapering (5% cosine taper), and filtering (0.2–10 Hz) were applied to seismic traces.

In addition, shallow lithological information (up to ~1000 m of the subsurface) was collected from the water exploration boreholes of the Bangladesh Water Development Board (BWDB) for areas surrounding each sensor location (Fig. 1). Though a borehole at the same site as the seismic observation is preferred, it is still helpful for setting initial values of the inversion parameter, especially thickness, and for addressing the problem of non-uniqueness of inversion. The lithological columns obtained from the boreholes in Zones1, 2, and 3 are illustrated in Figs. 3, 4, and 5, respectively.

Moreover, two-way travel time (TWTT) data of P-wave velocity (V_P) from the active seismic surveys of Bangladesh Petroleum Exploration Company Ltd. (BAPEX) at 15 locations near the seismic stations were utilized in this study. This information was particularly useful for the initial parameterization of the thickness and V_P values in the deeper portion of the profile along with addressing the ambiguity of non-uniqueness of inversion. Currently, we do not have permission to publish these data or disclose any information.

3.1. Computation of HVSR

From 15 days of continuous traces, an average HVSR curve from 0.2 to 10 Hz frequency range was computed for each station using the geopsy software (Wathelet et al., 2020). To remove energetic signals from the ASN data and improve the reliability of the measured HVSR spectra, the average amplitude ratio algorithm (an anti-triggering algorithm) with a short time to long time window (STA/LTA; Withers et al. (1998)) was imposed. Furthermore, the Konno-Ohmachi smoothing algorithm (Konno and Ohmachi, 1998), with smoothing a constant of 40, was applied to the Fourier amplitude spectra. The curve was computed using the total horizontal energy, as follows:

$$\frac{H}{V}(\omega) = \frac{\sqrt{H_1^2(\omega) + H_2^2(\omega)}}{V(\omega)} \quad (1)$$

where H_1 and H_2 stand for the Fourier amplitude spectra of the two horizontal components and V for that of the vertical component.

Fig. 6 includes examples of HVSR curves obtained from some of the stations in this study; the rest are provided in Supplementary Fig. S1. Among the stations in Zone 1, the fundamental frequency of the HVSR curve varies from approximately 0.8 Hz (FENC) to 7 Hz (JAFL) without any definite pattern from station to station. In Zone 2, fundamental

Table 1
General stratigraphy of Zone 1 (SB, modified and summarized from Alam et al. (2003)).

Age (Approx.)	Group	Formation	Thickness (max.) (m)	Lithology	Dep. Env.
Holocene		Alluvium	3350	Unconsolitaed to partly consolidated sand, silt, and clay with some gravels	Fluvial
Late Pleistocene	Dihing	Dihing		Unconsolidated to partly consolidated graveliferous deposits, both debris flow and braided stream	
Late Pliocene–Pleistocene	Dupi Tila	Upper		Clay and silty clay with fine to medium sandstone embedded as channels in clay	
		Lower		Fluvial medium to coarse grained sandstone with occasional pebbles	

Table 2
General stratigraphy of Zone 2 (BF, summarized and simplified from Alam et al. (2003) and Roy et al. (2012)).

Age	Group	Fromation	Thickness (max.) (m)	Lithology	Dep. Env.
Holocene			25	Alluvial silt, loose sand, and clay	Fluvial
Pleistocene		Madhupur Clay	25	Reddish silty clay and fluvial sand	
Plio-Pleistocene	Dupi Tila	Dupi Tila	400	Medium to fine grained loose sandstone with shale intercalations and coarse grained conglomerates	
		Girujan Clay	100	Bluish clay interbedded with silt and sand	
Pliocene	Tipam	Timap Sandstone	300	Sandstone with minor shale and clay beds	
Miocene	Surma	Boka Bil	1800	Alternation of shale and sandstone with siltstone interbeds	Marine to Deltaic

Table 3
General stratigraphy of Zone 3 (CTFB, summarized and simplified from Uddin and Lundberg (1999), Alam et al. (2003), and Rahman et al. (2016)).

Age	Group	Fromation	Thickness (max.) (m)	Lithology	Dep. Env.
Holocene		Alluvium	30	Alluvial silt, loose sand, and clay	Fluvial
Plio-Pleistocene	Dupi Tila	Dipi Tila	400	Sandstone with pebbles and gravel beds	
	Tipam	Girujan Clay	1300	Brown to blue mottled clay with calcareous nodules	
		Tipam Sandstone		Very coarse to fine sand with minor shale	
Miocene	Surma	Boka Bil	1600	Alternation of sand and shale	Marine to deltaic

frequency ranges from approximately 0.5 Hz (DHAK) to 1.8 Hz (CHNR). The fundamental frequencies of the stations in Zone 3 differ from approximately 2 Hz (LAMA) to 6 Hz (BRDL).

4. HVSR curve inversion

We utilized the HV-Inv (García-Jerez et al., 2016) software for our experimental HVSR curve inversion, in which the forward computation and inversion procedure of the HVSR curve is accomplished based on the DFA theory. Here, the full noise wavefield contribution (*i.e.*, both body and surface waves) is counted separately for full HVSR inversion, which is conducive to retrieving intricate and deeper structures. Moreover, the HVSR assumption based on the Rayleigh wave ellipticity or the SH wave transfer function is suitable for full HVSR inversion, but only around the predominant peak (Manea et al., 2020).

DFA theory considers the illumination of the relative power of each seismic state under the energy equipartition principle. Importantly, from DFA theory, we found that the autocorrelation in the frequency domain is proportional to the imaginary part of the three-dimensional (3D) elastodynamic GF when both the source and receiver are at the same point. Thus, the H*V*SR spectral ratio can be expressed in terms of the imaginary part of the GF:

$$\frac{H}{V}(x,\omega)=\sqrt{\frac{E_1(x,\omega)+E_2(x,\omega)}{E_3(x,\omega)}}=\sqrt{\frac{Im(G_{11}+G_{22})}{Im(G_{33})}} \tag{2}$$

where H_1 and H_2 denote the horizontal components, and V denotes the vertical component. For 3D-diffuse, equipartitioned, and harmonic displacement vector $u_i(\boldsymbol{x},\omega)$ within an elastic medium, the average autocorrelation of power spectral densities of motions at points $\boldsymbol{x_A}$ and $\boldsymbol{x_B}$ can be written as (Sánchez-Sesma et al., 2008):

$$\langle u_i(\boldsymbol{x}_A,\omega)u_j^*(\boldsymbol{x}_B,\omega)\rangle \propto Im\left[G_{ij}(\boldsymbol{x}_A,\boldsymbol{x}_B,\omega)\right] \tag{3}$$

where $\omega=2\pi f$ is the circular frequency; $u_i(\boldsymbol{x}_A,\omega)$ denotes the displacement field component in the i direction and at point $\boldsymbol{x}_A$; and $G_{ij}(\boldsymbol{x}_A,\boldsymbol{x}_B,\omega)$ represents the GF of displacement in the i direction at point $\boldsymbol{x}_A$ by a unit harmonic point force at $\boldsymbol{x}_B$ in the j direction. Here, the asterisk (*) represents the complex conjugate, and the angular brackets ($\langle\ \rangle$) indicate the azimuthal average. When both source and receiver coincide, *i.e.*, $\boldsymbol{x}_A=\boldsymbol{x}_B=\boldsymbol{x}$, and the respective components are the same, the DED $E_i(\boldsymbol{x},\omega)$ at point x could be shown to have the following form (Sánchez-Sesma et al., 2008):

$$\begin{aligned}E(\boldsymbol{x}_A)&=\rho\omega^2\langle u_m(\boldsymbol{x}_A)u_m^*(\boldsymbol{x}_A)\rangle\\&\propto Im[G_{mm}(\boldsymbol{x}_A,\boldsymbol{x}_A,\omega)]\end{aligned} \tag{4}$$

where ρ is the mass density.

The current inversion scheme requires five parameters as primary information: the layer thickness (h), V_P, V_S, density (ρ), and Poisson's ratio (v). The minimum number of layers for a site was selected by visually counting the number of peaks on the HVSR curve (Piña-Flores et al., 2017) along with the available subsurface information. The lower frequency peaks, particularly below 1 Hz, represent deeper layers, and Perton et al. (2020) have shown that a peak near 0.2 Hz is sensitive to the structure at approximately 6 km in the Los Angeles Basin. For the primary estimation of the layer thickness (h), along with available pre-existing information, that is, lithological information of BWDB and TWTT V_P information from BAPEX, we employed the equation $f_n=\frac{V_s}{4h}(2n+1)$ (Tuan et al., 2016; Molnar et al., 2022), where f_n is the frequency of a peak on the HVSR curve, h is the thickness of the layer, and n (= 0, 1, 2, …) is the mode number.

V_S velocity information for the intermediate depth has not been reported thus far in Bangladesh, except for Singh et al. (2016), who presented it with little resolution within 4 km at three stations (DHAK, MPUR and SUST) using receiver function inversion. Their one-dimensional (1D) profiles also include information on V_P/V_S ratio and density ρ. While setting the initial parameter space, the existing lithological information from lithologs of BWDB boreholes (Figs. 3– 5), stratigraphic information from the previous studies (*e.g.*, Alam et al., 2003), and the V_P information from BAPEX were considered in combination as constraints to address the non-uniqueness of the HVSR curve inversion solution. None of this information is from the exact location where the seismic sensors are located in a nearby area. Despite of this limitation, this initial information was extremely helpful during the initial parametrization. Furthermore, the density information of the sedimentary layers were taken from Singh et al. (2016), personal experience of geotechnical field and laboratory works of the authors of this article, and the published literatures (*e.g.*, Serajuddin et al., 2001; Hossain et al., 2020).

Several forward modellings were also performed to generate a good initial model for each station. As previously mentioned, the subsurface geomaterial distribution within the Bengal Basin is highly variable; therefore, models vary from station to station. An example of the parameterization for one station is presented in Table 4.

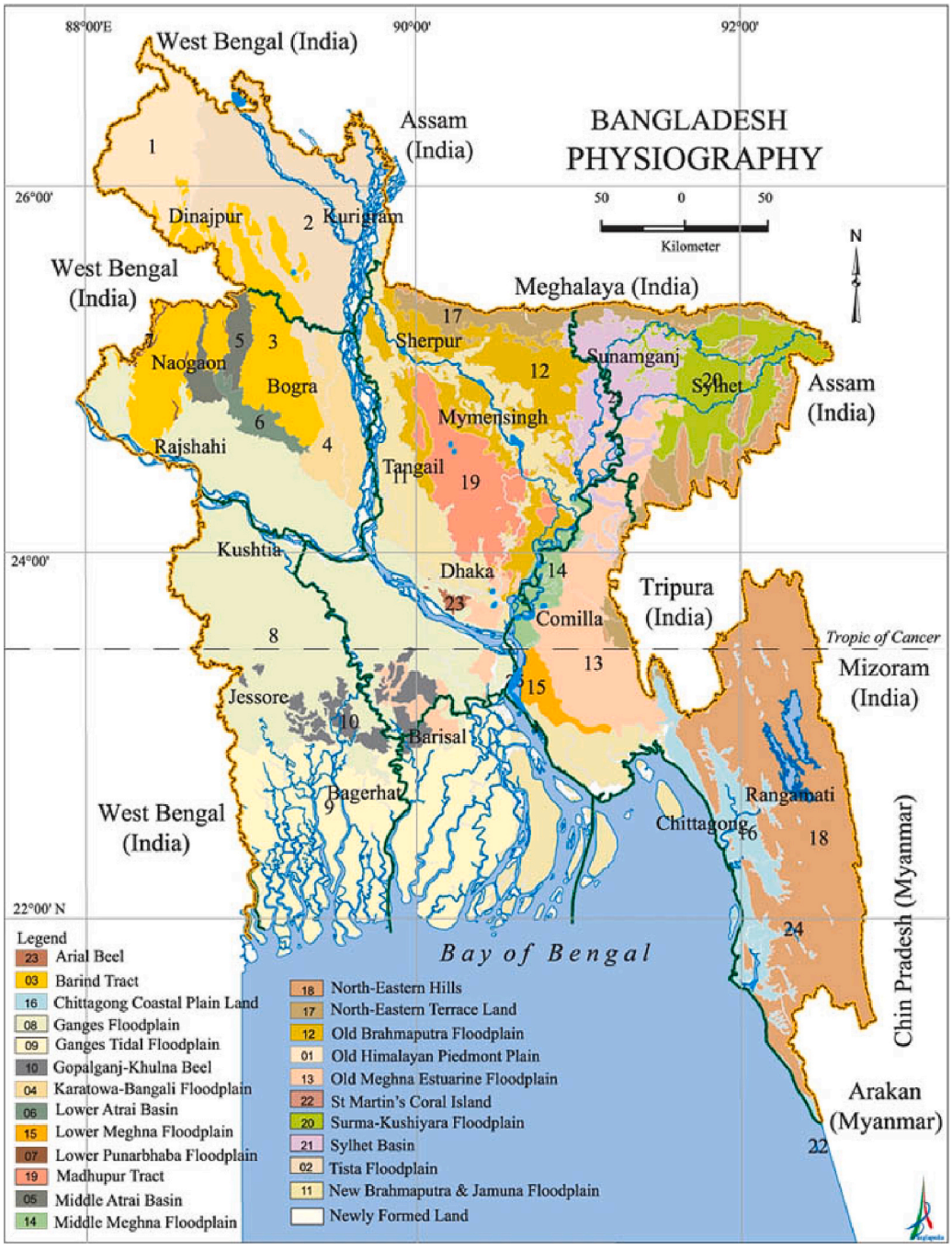

Fig. 2. Physiographic map of Bangladesh (Source: https://en.banglapedia.org/index.php/Physiography).

The theoretical HVSR curve computation in the inversion process begins with a random search within the parameter space using the non-linear Monte Carlo sampling method. The trial models from this point were then utilized to produce models using the linear downhill simplex method. After a number of iterations, the model with the lowest misfit value among the tested models was chosen as the best-fit model for the observed HVSR curve. The misfit function $E(m)$ is defined as (García-Jerez et al., 2016):

$$E(m) = \frac{1}{n}\sum_{j}^{n}\frac{\left(d_j^{obs} - d_j^{theo}(m)\right)^2}{\sigma_j^2} \tag{5}$$

where n is the number of frequency samples, d_j^{obs} denotes the observed value, d_j^{theo} denotes the theoretical value, and σ denotes standard deviation.

An example of an inversion result including the generated synthetic HVSR curves as well as the V_P, V_S, and density models is presented in Fig. 7 with misfit information, and such information for the rest of the stations is shown in Supplementary Figs. S2–S20. Herein, we considered the suggested best-fit profile after the conclusion of the inversion process to represent the V_S profile for each station. The underground V_S profiles of the stations in Zones 1, 2, and 3 are presented in Figs. 8–10, respectively.

The V_S velocities in Zone 1 (SB) vary from approximately 199 m/s (KNGT) to 448 m/s (FENC) at the surface. At the observed bottom, the V_S varies from approximately 916 m/s (BARL, depth of ~1550 m) to 1987 m/s (JAML, down to ~2800 m). However, at station JAFL, the velocity at the bottom is approximately 3222 m/s, at a depth of approximately

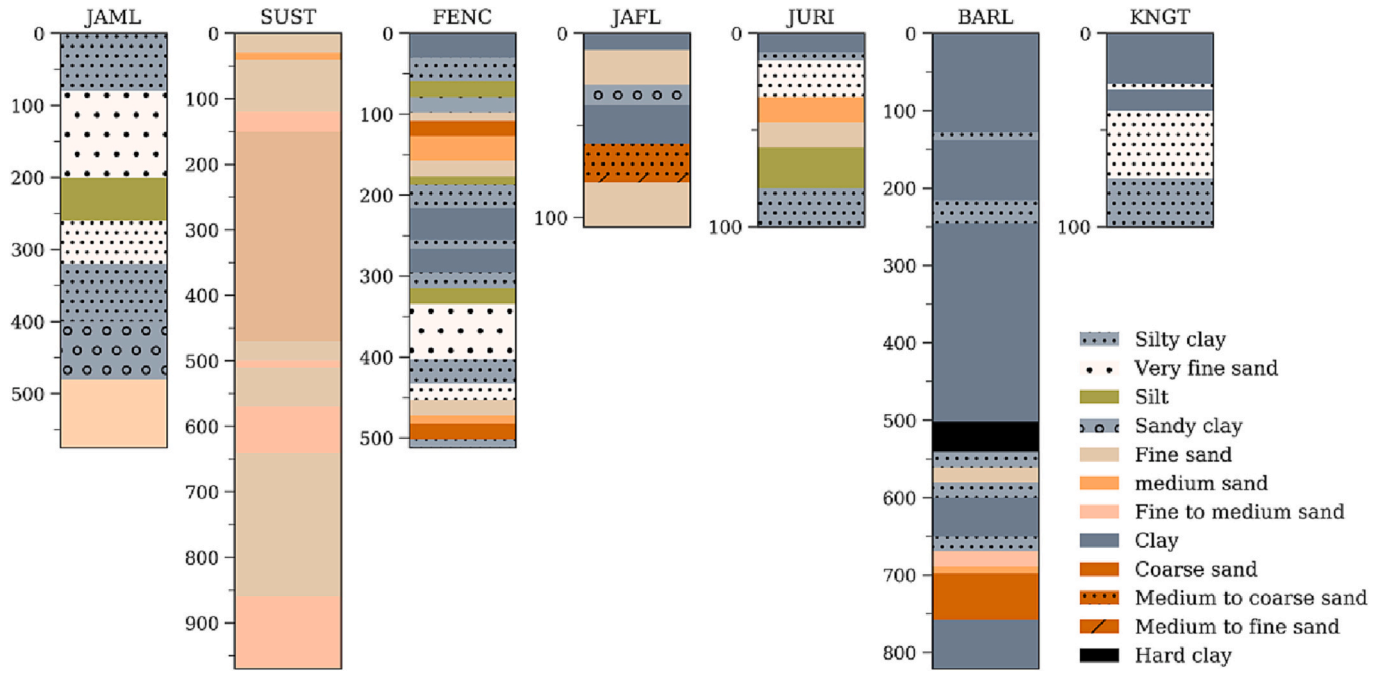

Fig. 3. Lithostratigraphic columns from BWDB boreholes in Zone 1. The vertical axis with each litholog indicates depth from the ground surface in meters. Locations of these logs can be found in Fig. 1.

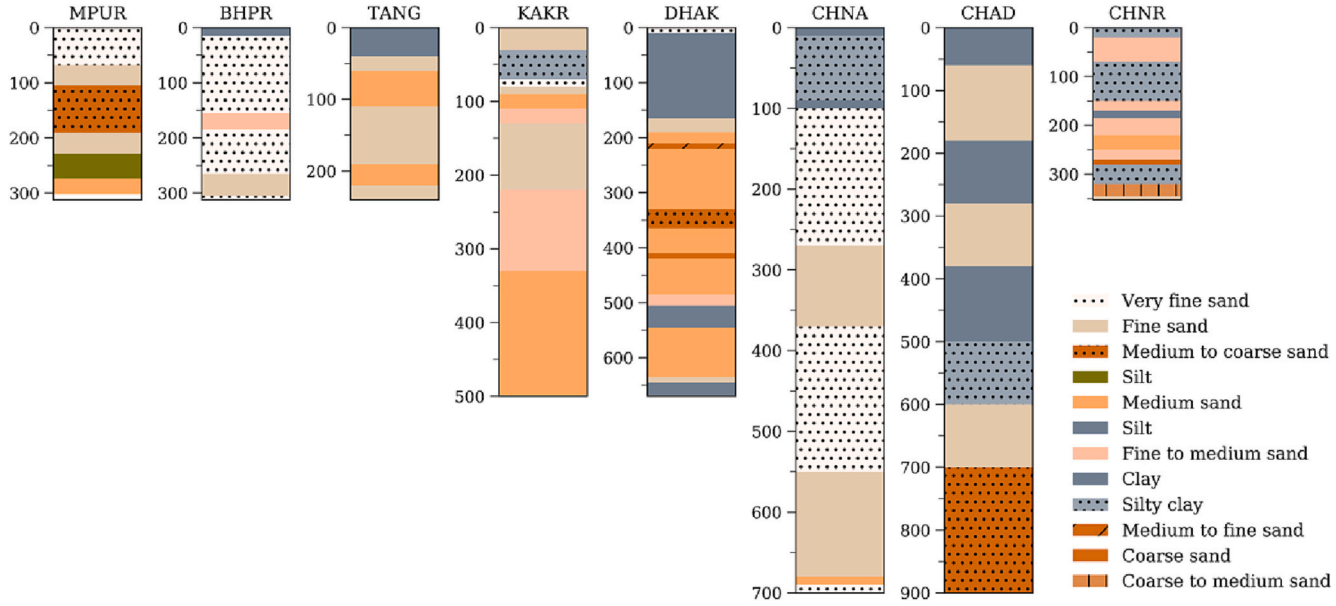

Fig. 4. Same as Fig. 3, but for Zone 2.

2800 m.

The V_S velocities in Zone 2 (BF) vary from approximately 64 m/s (BHPR) to 399 m/s (TANG) at the surface. At the observed bottom, the velocity ranges from approximately 723 m/s (MPUR, depth of ~2400 m) to 1300 m/s (CHNR, depth of ~1180 m).

The V_S velocities in Zone 3 (CTFB) vary from approximately 239 m/s (BAGH) to around 337 m/s (BARK) at the surface. At the observed bottom, this velocity ranges from approximately 657 m/s (BRDL, depth of ~2600 m) to 1547 m/s (LAMA, depth of ~2600 m). Many profiles exhibit low-velocity layers. The identified engineering bedrock positions are indicated in each profile in Figs. 8, 9, and 10. The spatial distribution of bedrock depths in the study area is presented in Fig. 11.

5. Seismic site response estimation

5.1. Site effect estimation at reference site SHL

Seismic site response analysis was performed at DHAK (Fig. 1) by computing the pseudo spectral acceleration (PSA), which we call the response spectra (RS), from a simulated earthquake recorded at reference site SHL in Shillong, Meghalaya, India (Fig. 1). First, by computing the HVSR, the reference site was confirmed to be a hard site (Lermo and Chávez-García, 1993). The Bengal Basin is experiencing subduction tectonics; hence, subduction zone earthquakes are relevant to this study. Therefore, we selected two subduction zone earthquakes in Nepal (Lizundia et al., 2017) recorded at SHL (Fig. 1). These two earthquakes,

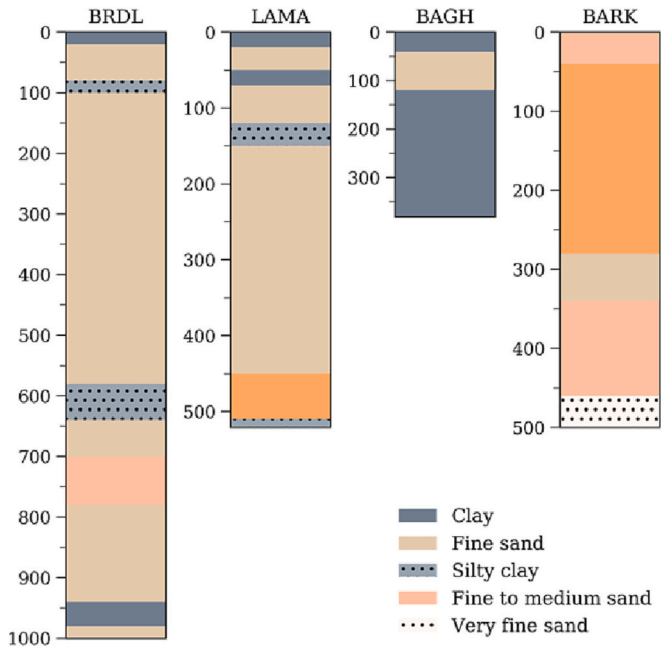

Fig. 5. Same as Fig. 3, but for Zone 3.

listed in Table 5, are considered as aftershocks of the M_W 7.8 Gorkha Nepal earthquake (Lizundia et al., 2017). However, the HVSR curves at the SHL were computed for both earthquakes (Fig. 12). The average HVSR curves exhibit no significant amplification of seismic waves for any of the earthquakes; thus, it was considered a hard site with negligible site effect.

5.2. Computation of response spectrum

RS was computed at site DHAK using the M_W 7.3 (2015-05-12, Table 5) subduction zone earthquake recorded on the EW component of SHL (Fig. 1). The site effect must be included in the simulated earthquake to estimate RS, which can be quantified by the vertically incident horizontally polarized SH wave transfer function (TF, Molnar et al., 2022). The manner in which each frequency of bedrock motion is amplified or deamplified by the soil deposit is quantified by TF. First, therefore, using the soil column information from this study (Fig. 9), TF was computed using the reflectivity method (Kennett and Kerry, 1979). The soil column information include the number of layers, layer thickness, V_P (m/s), V_S (m/s), density (kg/m^3), and quality factors for P- and S-waves (Q_P and Q_S, respectively). In this case, no attenuation was assumed. Thus, the TF we obtained was the Fourier transfer function for vertically propagating S-waves (Fig. 13).

Subsequently, a synthetic accelerogram (SA, Fig. 13) for site DHAK was generated from the simulation of a subduction zone earthquake (Table 5) recorded at a reference site (Fig. 1). This process involved the convolution of the earthquake spectrum with the TF in the frequency domain and then applying inverse Fourier transformation to obtain the SA. Thus, the site effect at DHAK was incorporated into SA.

Finally, from the SA, the RS was calculated using the Degtra program (Fig. 13), in which the displacement energy (E) of an oscillator is defined as follows:

Table 4
Example of parametrization for HVSR curve inversion at station DHAK.

Thickness (m) min–max	V_P (m/s)	V_S (m/s)	ρ (kg/m^3)	ν
	min–max	min–max	min–max	min–max
1–50	200–1500	50–918	1100–2600	0.20–0.49
2–50	200–900	80–500	1100–2600	0.20–0.49
10–50	200–1000	180–600	1100–2640	0.20–0.49
140–300	300–1200	500–693	1200–2600	0.25–0.49
200–600	1400–2000	770–1155	1300–2600	0.25–0.49
200–600	500–7000	200–2000	1300–2600	0.25–0.49
0	1400–7000	1000–3000	1300–3000	0.25–0.49

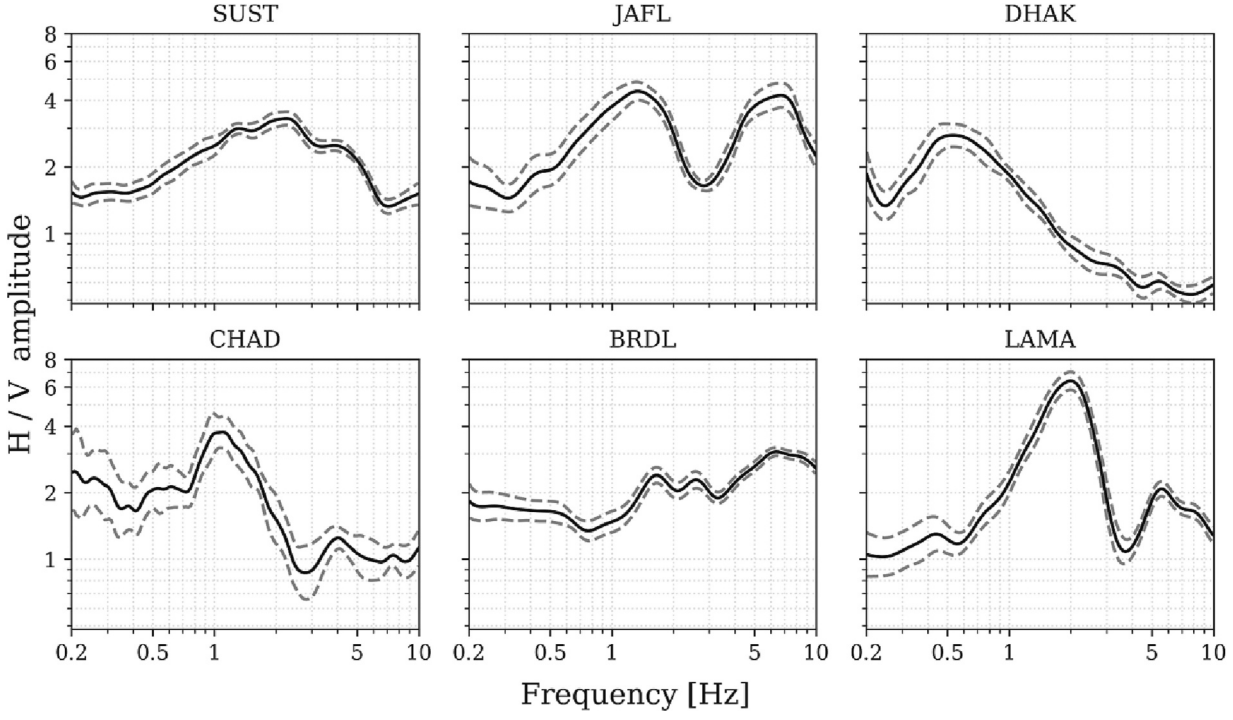

Fig. 6. Example of HVSR spectral ratio curves, showing two curves each from two stations in every zone. Gray dashed lines indicate the standard deviation from the average HVSR (solid black line). Zone 1: SUST and JAFL; Zone 2: DHAK and CHAD; Zone 3: BRDL and LAMA. Station names are indicated on the top of each panel.

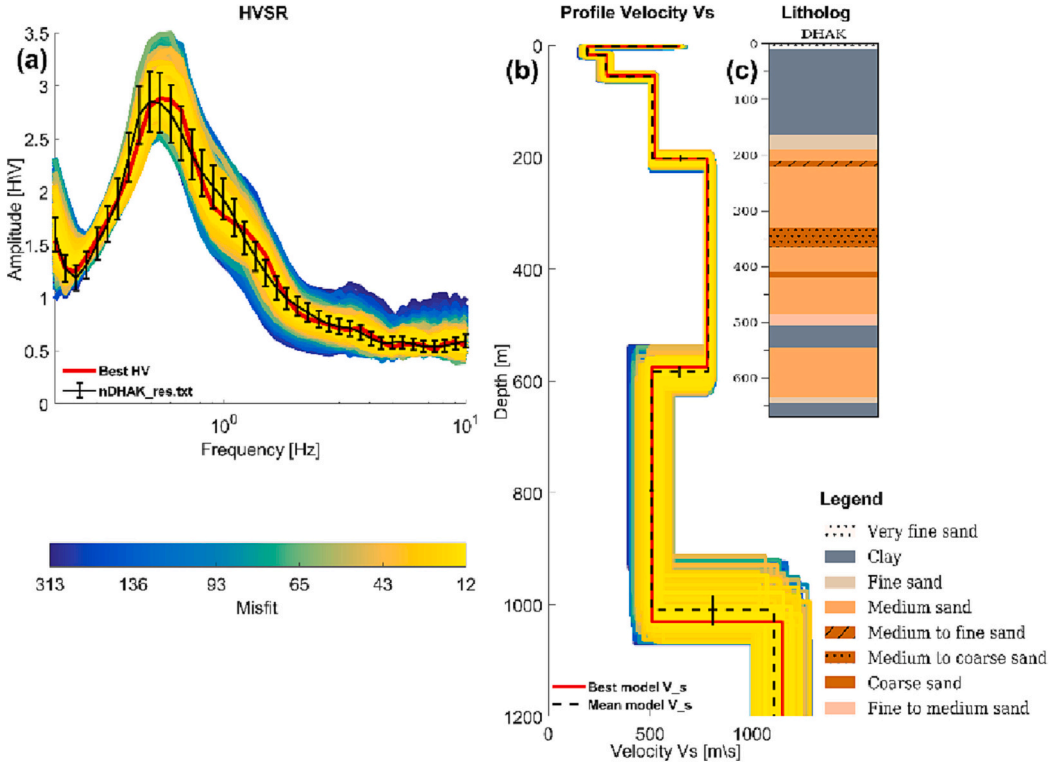

Fig. 7. Example of H/V curve inversion at station DHAK (situated in Dhaka, the capital city of Bangladesh), with a nearby borehole litholog (Fig. 1). (a) Experimental HVSR curve with generated models (b) Obtained V_S profile (c) Lithological column from BWDB borehole.

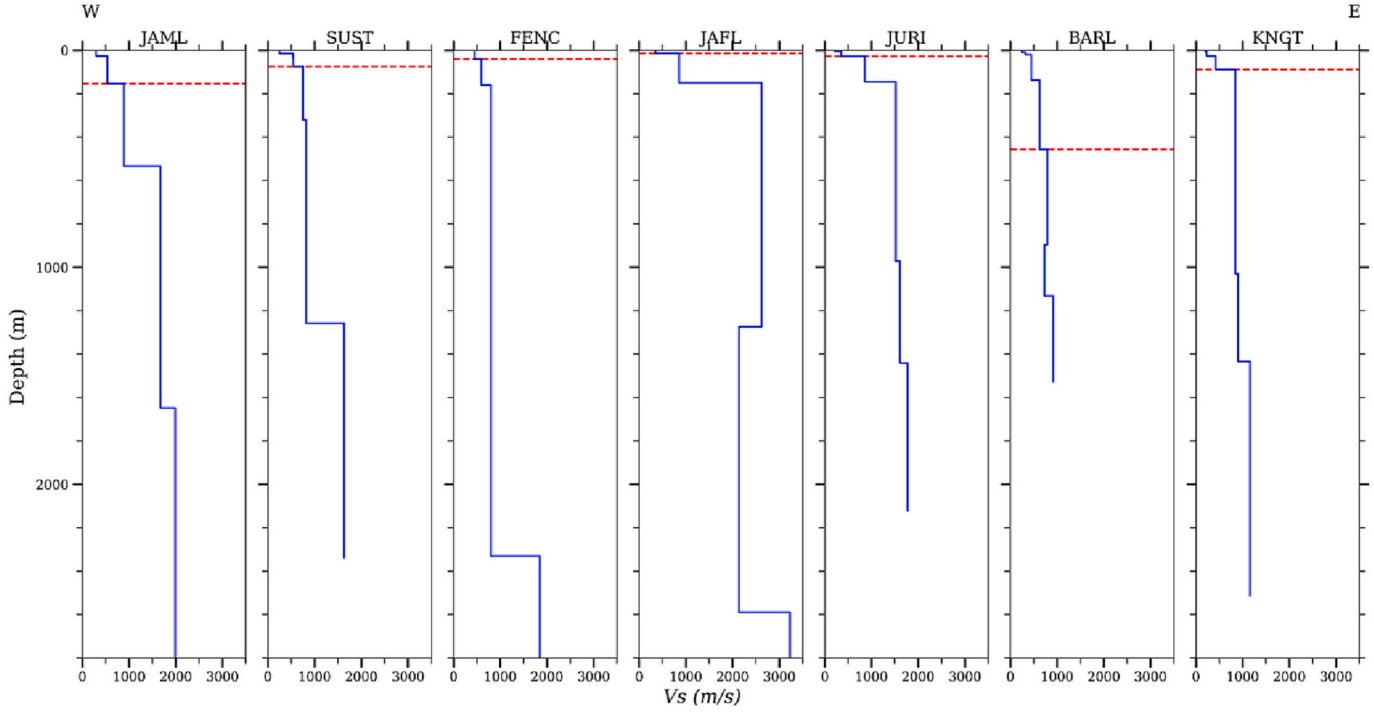

Fig. 8. Underground V_S velocity profile of each station of Zone 1 presented by solid blue line. The red dashed lines indicate the position of the engineering bedrock below a station. (For interpretation of the references to colour in this figure legend, the reader is referred to the web version of this article.)

$$E = \left| -m \int a(t)dx \right| \tag{6}$$

where m is the mass of the oscillator, $a(t)$ is the ground acceleration, and x is the relative oscillator displacement. The integral is performed for the selected period range of the accelerogram. The RS was estimated with 5% damping, which is representative of concrete and steel structures. The resultant displacement curve is presented in terms of acceleration, which is the PSA (RS). RS represents the seismic response spectrum of site DHAK.

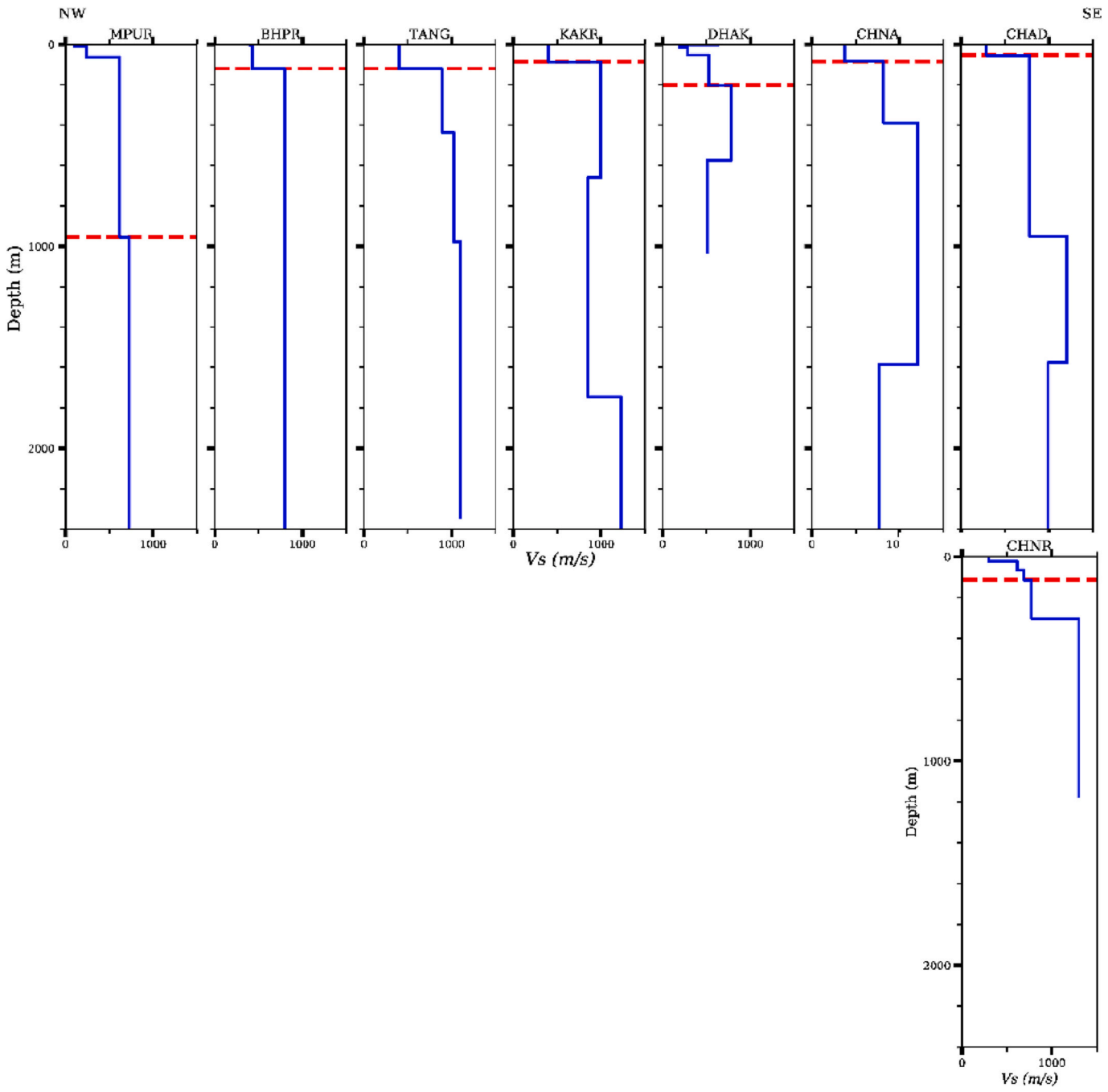

Fig. 9. Same as Fig. 8, but for Zone 2. Note that station CHNR is NE of the midpoint of the distribution of sensors in this zone.

6. Discussion

The dense and complex river network depicts the physiography of Bangladesh with floodplains and occasional piedmont alluvium deposits (Serajuddin et al., 2001). The tectonic activities led to two other dominant units, the Tertiary Hills and Uplifted Pleistocene Terraces, which were also severely dissected by the rivers (Serajuddin et al., 2001). However, this dense and complex river system forms an intriguing and rapidly variable subsurface geology (Small et al., 2009), for example, small sand pockets or channel deposits, pinchouts, abandoned channels or oxbow lake deposits, point bars, and levee deposits, rather than laterally continuous stratigraphy. In this context, the borehole lithologs (Figs. 3– 5) used in this study may not always be directly comparable to the inverted velocity profiles. Nonetheless, these lithologs provide useful insights into the shallow geological materials in the study area. Observations with a dense seismic network and boreholes are recommended for a particular locality of this region to obtain more reliable subsurface information.

6.1. The HVSR curves

In Zone 1 (SB), the HVSR curves exhibit the occurrence of the fundamental frequency peak both within the lower frequencies (below 1 Hz; JAML, FENC, and KNGT) and higher frequencies (above 2 Hz; SUST, JFL, JURI, and BARL). Double frequency peaks were observed at station JAFL, located in Jaflong. Jaflong is at the foothill of the uplifted Shillong Massif to the north, where broken rocks are deposited as gravel (Sarker, 2015). These piedmont deposits (Sarker, 2015) or the gravelliferous

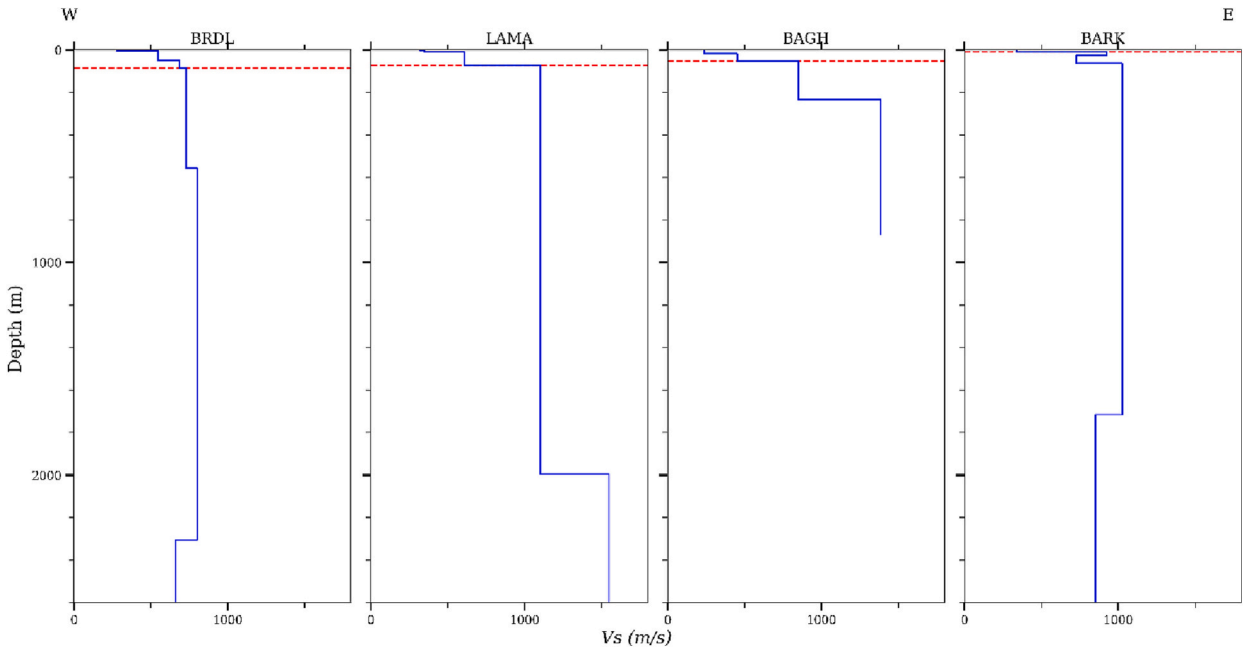

Fig. 10. Same as Fig. 8, but for Zone 3.

Dihing Formation (Roy et al., 2004) near the surface could have contributed to the higher frequency peak of the double frequency peaks; however, such lithology was not encountered in the BWDB borehole (Fig. 3). In the SB, subsided-basin and uplifted hillocks coexist (Hossain et al., 2020) and could render subsurface geology with either deep or shallow bedrock positions.

In Zone 2 (BF), all the HVSR curves show a fundamental frequency within approximately 0.5–1.8 Hz. Stations CHAD, CHNA, and CHNR were on the eastern side of the inferred plate boundary fault (Steckler et al., 2016), whereas the rest were on the western side. Apart from station KAKR (~1 Hz), all westerly stations have fundamental frequencies below 1 Hz. In contrast, the lowest fundamental frequency of the eastern stations is approximately 1 Hz.

In Zone 3 (CTFB), the fundamental frequency peaks were observed within a range of approximately 2–6 HZ, indicating shallow occurrences of the engineering bedrock. This is expected because the deep stratigraphic layers in this zone are exposed to the surface by continuous uplift as a result of the ongoing deformation along the Indo-Burmese subduction zone.

The Bengal Basin is filled by sedimentary successions deposited by the GBM river system, and their tributaries and distributaries make the subsurface conditions highly variable (Small et al., 2009). Therefore, the HVSR curves vary from station to station without any definite pattern.

6.2. S-wave profiles

Owing to highly varying subsurface conditions as well as observations from a sparse seismic network, no trend was observed in the S-wave velocity (V_S) profiles. However, this information could serve as an invaluable guideline for future exploration and seismic hazard mitigation studies in this region.

In Zone 1 (SB), the V_S velocities range from approximately 199 m/s at the surface to <2000 m/s at a depth of 2800 m, except at station JAFL, where at 2800 m, it is approximately 3200 m/s. As mentioned in the previous section, the higher velocity, particularly below station JAFL, could be related to the dominance of piedmont deposits in this area. In this zone, the observed velocity profile represents the Late Pliocene to Holocene sedimentary deposits (Table 1).

In Zone 2 (BF), The V_S velocities range from approximately 130 m/s on the surface to no >1400 m/s at a depth of approximately 2400 m. This zone exhibited lower velocities, likely because of deep soft sediments below the stations (Rahman et al., 2021). The observed depth indicates Miocene to Holocene sedimentary successions (Table 2).

In Zone 3 (CTFB), the V_S velocities vary from approximately 238 m/s at the surface to <1600 m/s at a depth of approximately 2600 m. This zone is highly deformed and uplifted and often shows ridges and valleys of anticlines. Thus, the near-surface materials of this area are dominated by the Holocene piedmont plain, alluvial valley fill deposits, and Tertiary sedimentary rocks (Rahman et al., 2016), which control the V_S velocity in this region. Here, the observed depth belongs to Miocene to Holocene sedimentary successions (Table 3). Several profiles contained low-velocity V_S zones, which could be related to water-saturated or petroleum-bearing zones.

6.3. Depth to engineering bedrock

Engineering bedrock (V_S > 760 m/s) depth has not been determined in the Bengal Basin, except for ten sites in Dhaka City by Rahman et al. (2021), who found bedrock at a depth of >175 m. Because of the widespread Holocene lowland floodplains and delta plains (Goodbred and Kuehl, 2000, Fig. 2), as well as the underlying Plio-Pleistocene fluvial deposits (Alam et al., 2003), thick soft sedimentary deposits (V_S > 760 m/s) are commonly present throughout the country. In such cases, V_S^{30} based site response analysis could be misleading (Rahman et al., 2021). Therefore, for an appropriate seismic site response estimation, it is necessary to know the depth of the bedrock. In this context, we present the bedrock depths from the estimated V_S profiles in this study (Figs. 8– 10). Full HVSR curve inversion based on the DFA theory of the full ASN wavefield facilitated the retrieval deep profiles. The bedrock depth at each station is also been presented in a map to comprehensively understand the spatial variability (Fig. 11).

In Zone 1 (SB), the engineering bedrock depth was mostly >30 m, that is, from approximately 40 m (FENC) to 455 m (BARL). However, at two stations, bedrock was found above 30 m, that is, 13 and 27 m, respectively, at JAFL and JURI. Station JAFL in Jaflong is on the foothill of the uplifted Shillong Massif, with piedmont deposits near the surface. Station JURI at Juri Upazila experienced Tertiary upliftment. The depth to bedrock at different locations indicates their existence within the Dihing to Dupi Tila Formations (Table 1). However, the variation in bedrock depth could be highly dependent on the local variation of

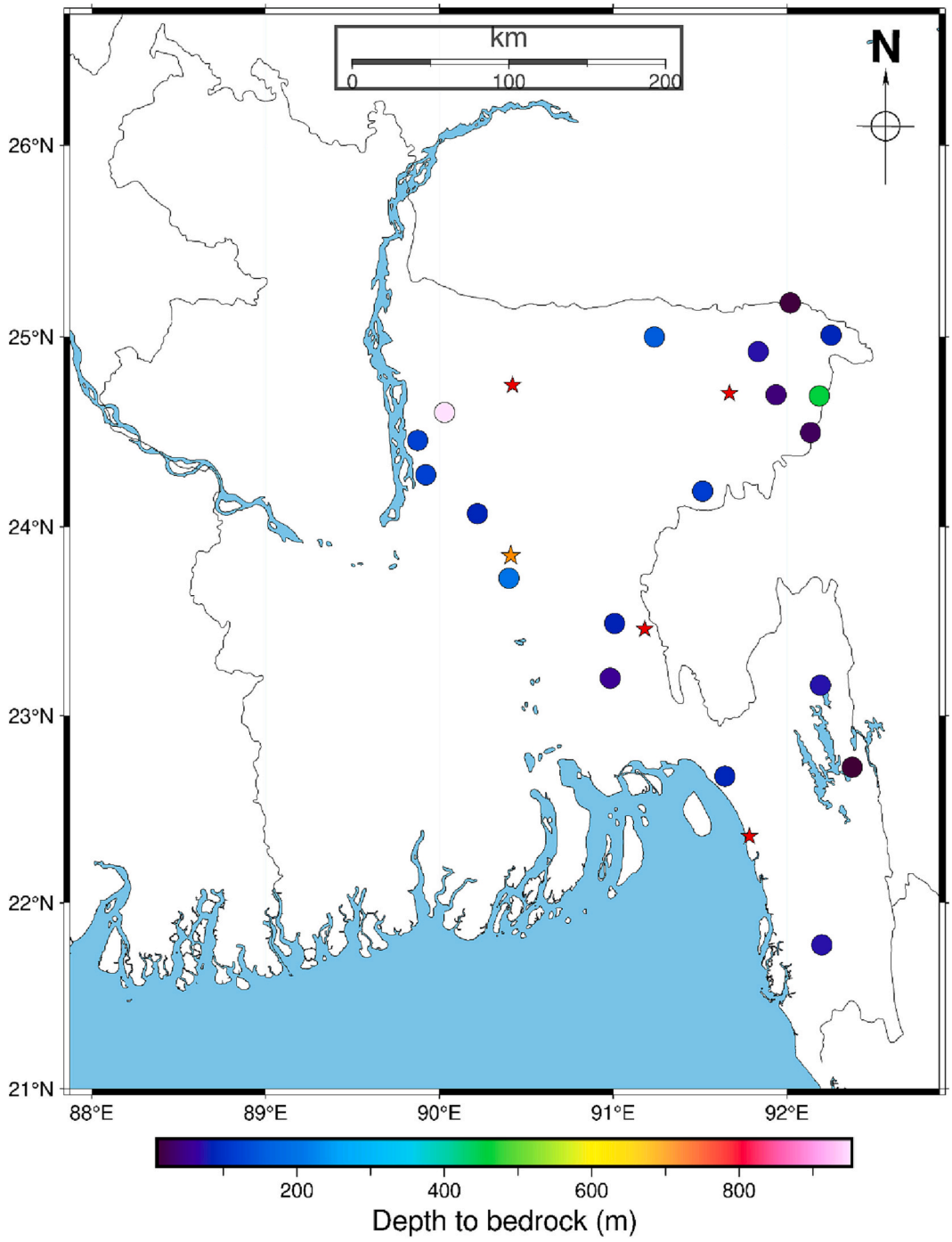

Fig. 11. Map showing the spatial distribution of the engineering bedrock depth in the studied region by colour scale. The orange colored star carries the same meaning as in Fig. 1. The red colored stars indicate some important cities within the study area. (For interpretation of the references to colour in this figure legend, the reader is referred to the web version of this article.)

Table 5
Description of the seismic events used for site effect estimation. Source: United States Geological Survey (https://earthquake.usgs.gov/earthquakes/search/).

Event date	GMT time	Latitude (^{O}N)	Longitude (°E)	Depth (km)	Magnitude (M_W)
2015-04-26	07:09:10	27.77	86.02	22.9	6.7
2015-05-12	07:05:19	27.81	86.07	15	7.3

subsurface geological materials.

In Zone 2 (BF), the bedrock depth varied from approximately 55 m (CHAD) to 953 m (MPUR). Notably, the stations west of the inferred megathrust (MPUR, BHPR, TANG, and DHAK) exhibit bedrock depths of >100 m, except station KAKR. In contrast, the easterly stations (CHNA and CHAD) of the inferred megathrust exhibit bedrock depths below 100 m. For another station, CHNR, bedrock was observed at a depth of approximately 114 m. Bedrock at all stations is situated within the depth corresponding to the Dupi Tila Formation, except at station MPUR (bedrock corresponding to the depth of the Tipam Formation, Table 2). At station DHAK, the only station in Dhaka City (the capital city of

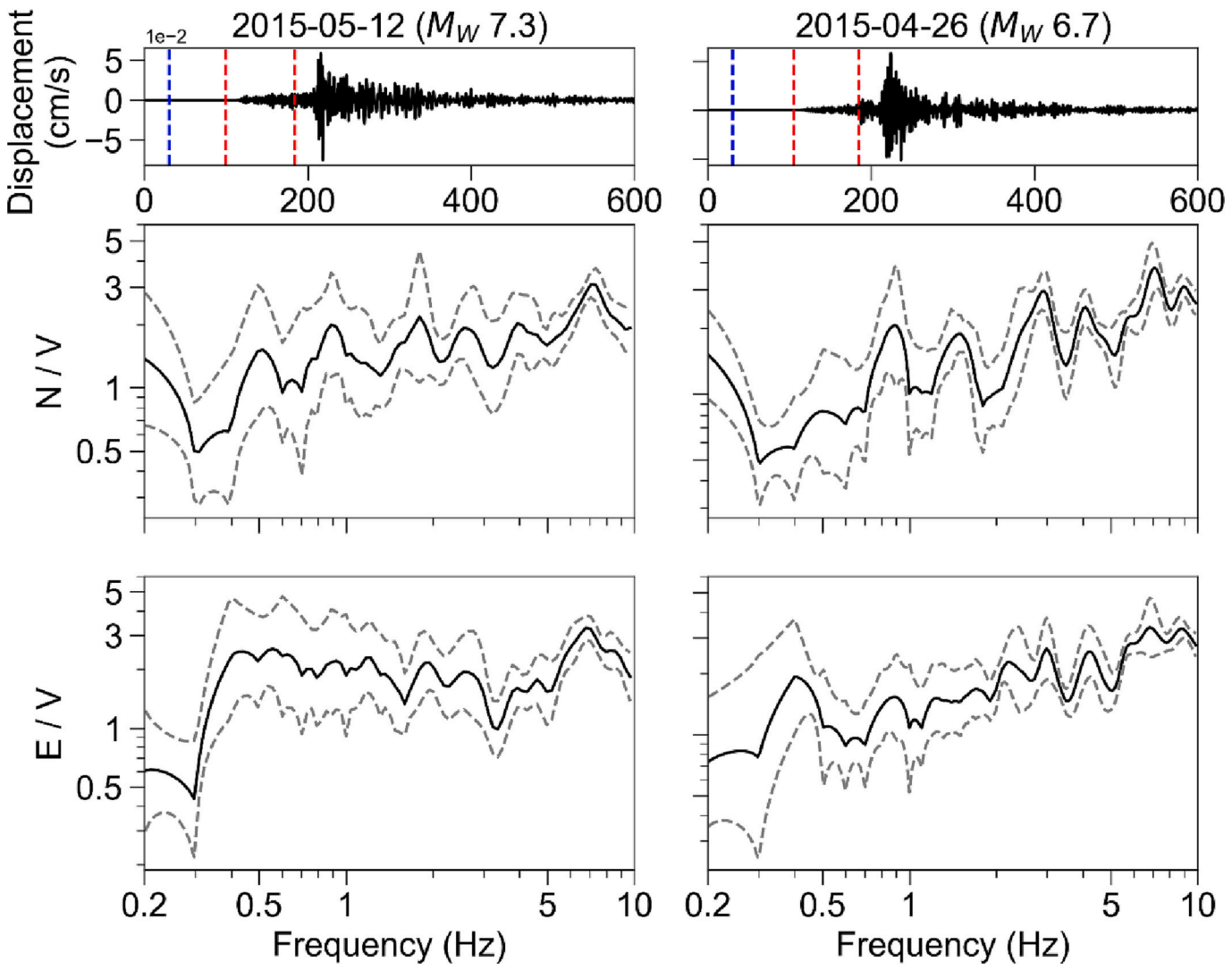

Fig. 12. HVSR as a function of frequency at reference station SHL. HVSR curves for the M_W 7.3 and 6.7 earthquakes are presented in the left and right columns, respectively. In each column, the vertical component of the earthquake record (filtered between 0.2 and 10 Hz) is at the top. Below are the HVSR curves for the NS and EW components, respectively. Blue dashed line: first arrival; red dashed lines: the S-wave portion of the earthquake used for HVSR computation; black solid line: average HVSR curve; gray dashed line: standard deviation of HVSR. (For interpretation of the references to colour in this figure legend, the reader is referred to the web version of this article.)

Bangladesh, Fig. 1), bedrock was found at a depth of approximately 194 m, which agrees with the findings of Rahman et al. (2021), who reported it at over 175 m.

The epicenters of the 1885 Bengal Earthquake (M_W 6.9) and 1918 Srimangal Earthquake (M_W 7.1) were approximately 100 km and 150 km from the center of the Dhaka City, respectively (Middlemiss, 1885; Rahman et al., 2021). However, little to no damage was reported for these events (Middlemiss, 1885; Stuart, 1921). In contrast, the 1897 Great Assam Earthquake (M_W 8.1) had its epicenter >200 km north of the city but caused severe damage to infrastructures (Oldham, 1899). These damage characteristics in Dhaka city suggest that the short-period seismic waves are de-amplified, whereas the long-period waves are amplified by the very thick and soft sedimentary deposits (Rahman et al., 2021).

The bedrock depth varied from approximately 72 m (LAMA) to 86 m (BRDL) in Zone 3 (CTFB), except at station BARK, where it was found at approximately 10 m. These bedrock depths could be correlated with the depth of the alluvium to the Dupi Tila Formation (Table 3). Because of deformation and uplift by ongoing subduction tectonics, deep rocks are exposed in many places in this zone. The shallow bedrock could be the result of the outcropping of deep rocks.

Deep bedrock may amplify long-period seismic waves from far-field sources and cause damage to high-rise buildings. Furthermore, the bedrock might be extremely shallow at sites in uplifted Pleistocene terrace deposits to amplify short-period seismic waves and may eventually cause damage to low-rise buildings for any possible nearby seismic sources (Rahman et al., 2021). However, in this study, such shallow bedrock was rarely found in the deep basin other than at some sites close to the uplifted Tertiary hills. Because of the rapidly varying surface and subsurface geology in the Bengal Basin, dense measurements are required to understand the geophysical bedrock depth for a particular area.

6.4. Site response at DHAK

To anticipate the effect of a large earthquake in the study area, a seismic site response analysis was performed by estimating the RS at a site (DHAK, in the capital city Dhaka, Bangladesh) based on a simulated subduction zone earthquake (M_W 7.3, Fig. 13) recorded at a reference site (Fig. 1). The engineering properties of several hundreds of meters of

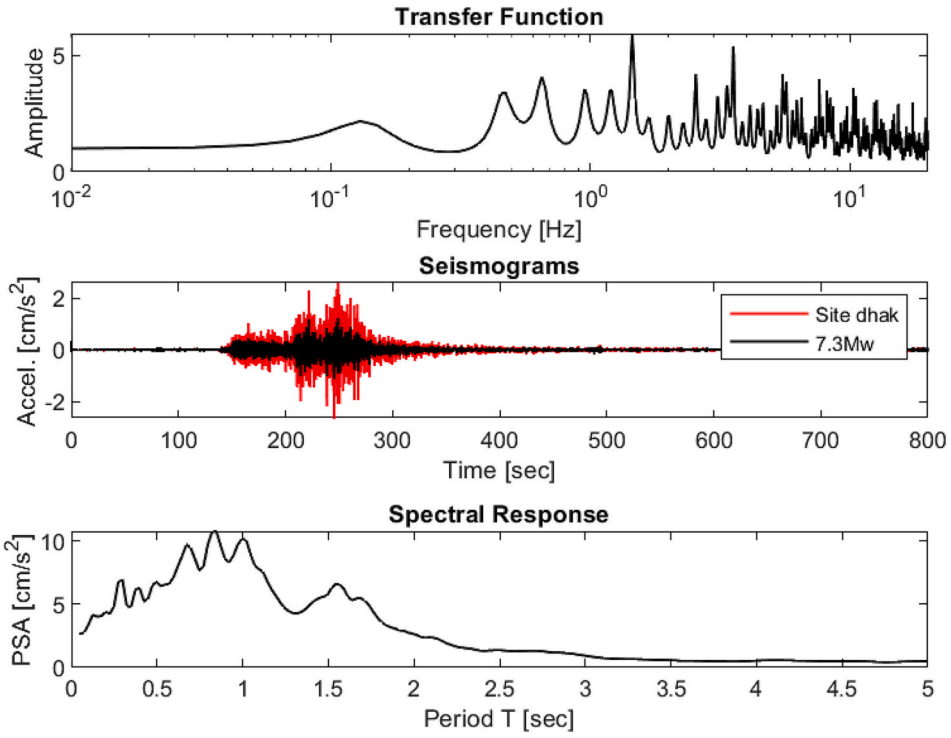

Fig. 13. Site response estimation at DHAK for the M_W 7.3 example earthquake recorded at reference site SHL. Top: TF estimated at DHAK. Middle: synthetic accelerogram at DHAK is superimposed on the observed accelerogram of the selected earthquake recorded on the EW component of SHL. Bottom: PSA (RS) at DHAK.

the subsurface, obtained from the H*V*SR curve inversion in this study (Fig. 9), were incorporated while simulating the earthquake. The SA shows that the maximum acceleration amplitude exceeds 2 cm/s^2 in the horizontal (EW) component. The RS shows that the predominant period of ground motion is from ~0.8–1 s, which agrees with several previous studies in Dhaka City (Islam et al., 2011; Rahman et al., 2021). Amplification over a longer period is expected in a sedimentary basin with thick soft sediments and may cause damage to multistory buildings due to a large earthquake (Rahman et al., 2021). A similar site response study for all the sites of this study and earthquakes from different directions at the reference site is beyond the scope of this article, but will be addressed in future work.

7. Conclusions

The 1D V_S velocity models at intermediate depths (maximum 2800 m) below 19 seismic stations were estimated in the Bengal Basin, Bangladesh by full HVSR analysis considering the full noise wavefield, constrained by available lithological and V_P information. From the V_S profiles, the engineering bedrock depth was also determined regionally in the Bengal Basin for the first time. The deep basin areas primarily exhibit deep bedrock positions below the ground surface, which may impose seismic risk for high-rise buildings. Shallow bedrock was predominantly related to uplifted areas owing to tectonic processes within the basin. The RS at DHAK, estimated by simulating a M_W 7.3 subduction zone earthquake, indicates that the predominant period of acceleration is within ~0.8–1 s, suggesting that multistory buildings may be at risk if subjected to ground motion of a large earthquake.

One of the uncertainties of this study is that neither the borehole lithologs nor the V_P profiles are located exactly at the seismic observation sites, and geological information may vary considerably within a few kilometers of the study area. Joint inversion with dispersion curves can increase the robustness of this type of study. Nonetheless, the V_S velocity profiles, along with information on engineering bedrock depth in a regional context could be useful preliminary guidelines for future exploration purposes, as well as seismic hazard and risk evaluation in Bangladesh. We recommend more dense seismic observation along with boreholes in each urban area of the country to properly assess the seismic risk. Moreover, future work includes site response estimation at all the sites of this study with the subsurface information derived herein from HVSR curve inversion and by simulating earthquakes from different directions at the reference site SHL.

CRediT authorship contribution statement

Atikul Haque Farazi: Conceptualization, Methodology, Writing – original draft, Visualization, Investigation, Formal analysis. **Md. Shakhawat Hossain:** Conceptualization, Funding acquisition, Project administration, Data curation, Validation, Writing – review & editing. **Yoshihiro Ito:** Supervision, Writing – review & editing. **José Piña-Flores:** Validation, Formal analysis, Methodology, Software, Visualization. **A.S.M. Maksud Kamal:** Supervision, Funding acquisition, Project administration. **Md. Zillur Rahman:** Supervision, Funding acquisition, Project administration.

Declaration of Competing Interest

The authors declare that they have no known competing financial interests or personal relationships that could have appeared to influence the work reported in this paper.

Data availability

The seismic data are freely available on the IRIS website. The lithologs from BWDB can be acquired by contacting BWDB in a proper manner. The TWTT P-wave data of BAPEX may be available upon request.

Acknowledgements

We are thankful to the Ministry of Science and Technology, Bangladesh for funding this project (grant number GO:39.00.0000.009.06.024.19/ES-322-338 (SL. 294, Gr. SL. 322 ES), dated: January 12, 2020). We are also indebted to Md. Jakir Hossain and BWDB for providing borehole lithologs. We are indebted to BAPEX for providing TWTT P-wave data. Degtra 4 program of Mario Ordaz was used for computing Response Spectrum. We are grateful to Dr. Hiroshi Kawase and Dr. Sinichi Matsushima, professors at the Disaster Prevention Research Institute (DPRI), Kyoto University, for their valuable suggestions during this work. We would like to express our deep gratitude to Dr. Francisco José Sánchez-Sesma, Professor, Institute of Engineering, National Autonomous University of Mexico, for his valuable advice on improving this manuscript. We are grateful to Dr. Emmanuel Soliman M. Garcia, Postdoctoral Fellow, DPRI, Kyoto University, for kindly helping improve the language of the manuscript. We are grateful to the two anonymous reviewers for their valuable suggestions for improving the manuscript.

Appendix A. Supplementary data

Supplementary data to this article can be found online at https://doi.org/10.1016/j.jappgeo.2023.104967.

References

Aki, K., 1957. Space and time spectra of stationary stochastic waves, with special reference to microtremors. Bull. Earthq. Res. Inst. 35, 415–457. Retrieved from. https://ci.nii.ac.jp/naid/10003122622.

Alam, M., Alam, M.M., Curray, J.R., Chowdhury, M.L.R., Gani, M.R., 2003. An overview of the sedimentary geology of the Bengal Basin in relation to the regional tectonic framework and basin-fill history. Sediment. Geol. 155, 179–208. https://doi.org/10.1016/S0037-0738(02)00180-X.

Arai, H., Tokimatsu, K., 2004. S-Wave Velocity Profiling by Inversion of Microtremor H/V Spectrum. Bull. Seismol. Soc. Am. 94, 53–63. https://doi.org/10.1785/0120030028.

Asten, M.W., Askan, A., Ekincioglu, E.E., Sisman, F.N., Ugurhan, B., 2014. Site characterisation in North-Western Turkey based on SPAC and HVSR analysis of microtremor noise. Explor. Geophys. 45, 74–85. https://doi.org/10.1071/EG12026.

Bajaj, K., Anbazhagan, P., 2019. Seismic site classification and correlation between VS and SPT-N for deep soil sites in Indo-Gangetic Basin. J. Appl. Geophys. 163, 55–72. https://doi.org/10.1016/j.jappgeo.2019.02.011.

Bilham, R., 2004. Earthquakes in India and the Himalaya: Tectonics, geodesy and history. Ann. Geophys. 47, 839–858. https://doi.org/10.4401/ag-3338.

Bonnefoy-Claudet, S., Cotton, F., Bard, P.-Y., 2006. The nature of noise wavefield and its applications for site effects studies. Earth-Science Rev. 79, 205–227. https://doi.org/10.1016/j.earscirev.2006.07.004.

Bürgi, P., Hubbard, J., Akhter, S.H., Peterson, D.E., 2021. Geometry of the Décollement Below Eastern Bangladesh and Implications for Seismic Hazard. J. Geophys. Res. Solid Earth 126. https://doi.org/10.1029/2020JB021519 e2020JB021519.

Davies, C., Best, J., Collier, R., 2003. Sedimentology of the Bengal shelf, Bangladesh: Comparison of late Miocene sediments, Sitakund anticline, with the modern, tidally dominated shelf. Sediment. Geol. 155, 271–300. https://doi.org/10.1016/S0037-0738(02)00183-5.

Fäh, D., Kind, F., Giardini, D., 2003. Inversion of local S-wave velocity structures from average H/V ratios, and their use for the estimation of site-effects. Journal of Seismology 7, 449–467. https://doi.org/10.1023/B:JOSE.0000005712.86058.42.

Farazi, A.H., Ito, Y., Garcia, E.S.M., Lontsi, A.M., Sánchez-Sesma, F.J., Jaramillo, A., Ohyanagi, S., et al., 2023. Shear-wave velocity structure at the Fukushima forearc region based on H/V analysis of ambient noise recordings by ocean bottom seismometers. Geophys. J. Int. https://doi.org/10.1093/gji/ggad028.

García-Jerez, A., Piña-Flores, J., Sánchez-Sesma, F.J., Luzón, F., Perton, M., 2016. A computer code for forward calculation and inversion of the H/V spectral ratio under the diffuse field assumption. Comput. Geosci. 97, 67–78. https://doi.org/10.1016/j.cageo.2016.06.016.

Goodbred, S.L., Kuehl, S.A., 2000. The significance of large sediment supply, active tectonism, and eustasy on margin sequence development: Late Quaternary stratigraphy and evolution of the Ganges–Brahmaputra delta. Sediment. Geol. 133, 227–248. https://doi.org/10.1016/S0037-0738(00)00041-5.

Goodbred, Steven L., Kuehl, S.A., Steckler, M.S., Sarker, M.H., 2003. Controls on facies distribution and stratigraphic preservation in the Ganges-Brahmaputra delta sequence. Sediment. Geol. 155, 301–316. https://doi.org/10.1016/S0037-0738(02)00184-7.

Hossain, M.S., Kamal, A.S.M.M., Rahman, M.Z., Farazi, A.H., Mondal, D.R., Mahmud, T., Ferdous, N., 2020. Assessment of soil liquefaction potential: a case study for Moulvibazar town, Sylhet, Bangladesh. SN Appl. Sci. 2 https://doi.org/10.1007/s42452-020-2582-x.

Islam, S.A.B.M., Jameel, M., Ahmad, S.I., Salman, F.A., Jummat, M.Z., 2011. Engendering earthquake response spectra for Dhaka region usable in dynamic analysis of structures. Sci. Res. Essays 6, 3519–3530. https://doi.org/10.5897/SRE11.218.

Johnson, S.Y., Alam, A.M.N., 1991. Sedimentation and tectonics of the Sylhet trough, Bangladesh. Geol. Soc. Am. Bull. 103, 1513. https://doi.org/10.1130/0016-7606(1991)103<1513:SATOTS>2.3.CO;2.

Kennett, B.L.N., Kerry, N.J., 1979. Seismic waves in a stratified half space. Geophys. J. Int. 57, 557–583. https://doi.org/10.1111/J.1365-246X.1979.TB06779.X.

Khan, A.A., Chouhan, R.K.S., 1996. The crustal dynamics and the tectonic trends in the Bengal Basin. J. Geodyn. 22, 267–286. https://doi.org/10.1016/0264-3707(96)00022-1.

Konno, K., Ohmachi, T., 1998. Ground-motion characteristics estimated from spectral ratio between horizontal and vertical components of microtremor. Bull. Seismol. Soc. Am. 88, 228–241. https://doi.org/10.1785/BSSA0880010228.

Lacoss, R.T., Kelly, E.J., Toksöz, M.N., 1969. ESTIMATION OF SEISMIC NOISE STRUCTURE USING ARRAYS. GEOPHYSICS 34, 21–38. https://doi.org/10.1190/1.1439995.

Lermo, J., Chávez-García, F.J., 1993. Site effect evaluation using spectral ratios with only one station. Bull. Seismol. Soc. Am. 83, 1574–1594. https://doi.org/10.1785/BSSA0830051574.

Lizundia, B., Davidson, R.A., Hashash, Y.M.A., Olshansky, R., 2017. Overview of the 2015 Gorkha, Nepal, Earthquake and the Earthquake Spectra Special Issue. Earthq. Spectra 33, S1–S20. https://doi.org/10.1193/120817EQS252M/ASSET/IMAGES/LARGE/10.1193_120817EQS252M-FIG 2.JPEG.

Lontsi, A.M., Sánchez-Sesma, F.J., Molina-Villegas, J.C., Ohrnberger, M., Krüger, F., 2015. Full microtremor H/V(z,f) inversion for shallow subsurface characterization. Geophys. J. Int. 202, 298–312. https://doi.org/10.1093/gji/ggv132.

Lontsi, A.M., Ohrnberger, M., Krüger, F., Sánchez-Sesma, F.J., 2016. Combining surface-wave phase-velocity dispersion curves and full microtremor horizontal-to-vertical spectral ratio for subsurface sedimentary site characterization. Interpretation 4, SQ41–SQ49. https://doi.org/10.1190/INT-2016-0021.1.

Mahmud, M.I., Mia, A.J., Islam, M.A., Peas, M.H., Farazi, A.H., Akhter, S.H., 2020. Assessing bank dynamics of the Lower Meghna River in Bangladesh: an integrated GIS-DSAS approach. Arab. J. Geosci. 13, 602. https://doi.org/10.1007/s12517-020-05514-4.

Manea, E.F., Cioflan, C.O., Coman, A., Michel, C., Poggi, V., Fäh, D., 2020. Estimating Geophysical Bedrock Depth using Single Station Analysis and Geophysical Data in the Extra-Carpathian Area of Romania. Pure Appl. Geophys. 177, 4829–4844. https://doi.org/10.1007/s00024-020-02548-3.

Maranò, S., Reller, C., Loeliger, H.-A., Fäh, D., 2012. Seismic waves estimation and wavefield decomposition: application to ambient vibrations. Geophys. J. Int. 191, 175–188. https://doi.org/10.1111/j.1365-246X.2012.05593.x.

Middlemiss, C., 1885. Report on the Bengal Earthquake of July 14, 1885., Dhaka.

Molnar, P., Tapponnier, P., 1975. Cenozoic tectonics of Asia: Effects of a continental collision. Science (80-.) 189, 419–426. https://doi.org/10.1126/SCIENCE.189.4201.419/ASSET/758EDFC9-BD00-4956-96EA-CF94D64B411E/ASSETS/SCIENCE.189.4201.419.FP.PNG.

Molnar, S., Cassidy, J.F., Castellaro, S., Cornou, C., Crow, H., Hunter, J.A., Matsushima, S., et al., 2018. Application of Microtremor Horizontal-to-Vertical Spectral Ratio (MHVSR) analysis for Site Characterization: State of the Art. Surv. Geophys. 39, 613–631. https://doi.org/10.1007/s10712-018-9464-4.

Molnar, S., Sirohey, A., Assaf, J., Bard, P.Y., Castellaro, S., Cornou, C., Cox, B., et al., 2022. A review of the microtremor horizontal-to-vertical spectral ratio (MHVSR) method. J. Seismol. 3, 1–33. https://doi.org/10.1007/S10950-021-10062-9/FIGURES/10.

Nakamura, Y., 1989. A method for dynamic characteristics estimation of subsurface using microtremor on the ground surface. Railw. Tech. Res. Inst. Q. Rep. 30, 25–33. Retrieved from. https://trid.trb.org/view/294184.

Nakamura, Y., 2000. Clear identification of fundamental idea of Nakamura's technique and its applications. Spectrum 2656. Retrieved from. http://www.sdr.co.jp/papers/n_tech_and_application.pdf.

Ni, J.F., Guzman-Speziale, M., Bevis, M., Holt, W.E., Wallace, T.C., Seager, W.R., 1989. Accretionary tectonics of Burma and the three-dimensional geometry of the Burma subduction zone. Geology 17, 68. https://doi.org/10.1130/0091-7613(1989)017<0068:ATOBAT>2.3.CO;2.

Oldham, R., 1899. Report of the Great Earthquake of 12th June, 1897. Office of the Geological Survey, Calcutta.

Perton, M., Spica, Z.J., Clayton, R.W., Beroza, G.C., 2020. Shear wave structure of a transect of the Los Angeles basin from multimode surface waves and H/V spectral ratio analysis. Geophys. J. Int. 220, 415–427. https://doi.org/10.1093/gji/ggz458.

Piña-Flores, J., Perton, M., García-Jerez, A., Carmona, E., Luzón, F., Molina-Villegas, J. C., Sánchez-Sesma, F.J., 2017. The inversion of spectral ratio H/V in a layered system using the diffuse field assumption (DFA). Geophys. J. Int. 208, 577–588. https://doi.org/10.1093/gji/ggw416.

Rahman, M.Z., Siddiqua, S., Kamal, A.S.M.M., 2016. Shear wave velocity estimation of the near-surface materials of Chittagong City, Bangladesh for seismic site characterization. J. Appl. Geophys. 134, 210–225. https://doi.org/10.1016/j.jappgeo.2016.09.006.

Rahman, M.Z., Hossain, M.S., Kamal, A.S.M.M., Siddiqua, S., Mustahid, F., Farazi, A.H., 2018. Seismic site characterization for Moulvibazar town, Bangladesh. Bull. Eng. Geol. Environ. 77, 1451–1471. https://doi.org/10.1007/s10064-017-1031-6.

Rahman, M.Z., Siddiqua, S., Kamal, A.S.M.M., 2021. Site response analysis for deep and soft sedimentary deposits of Dhaka City, Bangladesh. Nat. Hazards 106, 2279–2305. https://doi.org/10.1007/s11069-021-04543-w.

Roy, M.K., Karmakar, B.C., Saha, S., Chaudhuri, S., 2004. Facies and Depositional Environment of the Dupitila Formation, Dupitila Hill Range, Jaintiapur, Sylhet, Bangladesh. Geol. Soc. India 63, 139–157. Retrieved from. http://www.geosocindia.org/index.php/jgsi/article/view/82970.

Roy, M.K., Ahmed, S.S., Bhattacharjee, T.K., Mahmud, S., Moniruzzaman, M., Masidul Haque, M., Saha, S., et al., 2012. Paleoenvironment of deposition of the Dupi Tila Formation, Lalmai Hills, Comilla, Bangladesh. J. Geol. Soc. India 80, 409–419. https://doi.org/10.1007/s12594-012-0159-z.

Sadiq, M., Umrao, R.K., Sharma, B.B., Chakraborti, S., Bhattacharyya, S., Kundu, A., 2018. Mineralogy, geochemistry and geochronology of mafic magmatic enclaves and their significance in evolution of Nongpoh granitoids, Meghalaya, NE India. Geol. Soc. Spec. Publ. 463, 171–198. https://doi.org/10.1144/SP463.2.

Sánchez-Sesma, F.J., Pérez-Ruiz, J.A., Luzón, F., Campillo, M., Rodríguez-Castellanos, A., 2008. Diffuse fields in dynamic elasticity. Wave Motion 45, 641–654. https://doi.org/10.1016/J.WAVEMOTI.2007.07.005.

Sánchez-Sesma, F.J., Rodríguez, M., Iturrarán-Viveros, U., Luzón, F., Campillo, M., Margerin, L., García-Jerez, A., et al., 2011. A theory for microtremor H/V spectral ratio: Application for a layered medium. Geophys. J. Int. 186, 221–225. https://doi.org/10.1111/j.1365-246X.2011.05064.x.

Sarker, M.N., 2015. Gravel deposits of Dauki-Piyan River Bed and Surrounding Flood Plains: a case study. J. Asiat. Soc. Bangladesh 41, 225–232. Retrieved from. https://www.asiaticsociety.org.bd/journal/S_Dec_2015/9.pdf.

Serajuddin, M., Hai, M.A., Hossain, M.J., Islam, M.M., 2001. Characterization of Uplifted Pleistocene Deposits in Dhaka City. J. Civ. Eng. 29, 167–186.

Shapiro, N.M., Campillo, M., Stehly, L., Ritzwoller, M.H., 2005. High-Resolution Surface-Wave Tomography from Ambient Seismic Noise. Science (80-.) 307, 1615–1618. https://doi.org/10.1126/science.1108339.

Singh, A., Bhushan, K., Singh, C., Steckler, M.S., Akhter, S.H., Seeber, L., Kim, W.Y., et al., 2016. Crustal structure and tectonics of Bangladesh: New constraints from inversion of receiver functions. Tectonophysics 680, 99–112. https://doi.org/10.1016/j.tecto.2016.04.046.

Small, C., Steckler, M., Seeber, L., Akhter, S.H., Goodbred, S., Mia, B., Imam, B., 2009. Spectroscopy of sediments in the Ganges–Brahmaputra delta: Spectral effects of moisture, grain size and lithology. Remote Sens. Environ. 113, 342–361. https://doi.org/10.1016/j.rse.2008.10.009.

Steckler, M.S., Akhter, S.H., Seeber, L., 2008. Collision of the Ganges-Brahmaputra Delta with the Burma Arc: Implications for earthquake hazard. Earth Planet. Sci. Lett. 273, 367–378. https://doi.org/10.1016/j.epsl.2008.07.009.

Steckler, M.S., Mondal, D.R., Akhter, S.H., Seeber, L., Feng, L., Gale, J., Hill, E.M., et al., 2016. Locked and loading megathrust linked to active subduction beneath the Indo-Burman Ranges. Nat. Geosci. 9, 615–618. https://doi.org/10.1038/ngeo2760.

Stuart, C.D., 1921. The Srimangal Earthquake of 8th July, 1918. By Murray Stuart, D.SC. Mem. Geol. Surv. India, vol. xlvi, 1920. pp. 1–70, 12 plates. Geol. Mag. 58, 281–282. Cambridge University Press (CUP). https://doi.org/10.1017/s001675680009097x.

Tuan, T.T., Vinh, P.C., Malischewsky, P., Aoudia, A., 2016. Approximate Formula of Peak Frequency of H/V Ratio Curve in Multilayered Model and its use in H/V Ratio Technique. Pure Appl. Geophys. 173, 487–498. https://doi.org/10.1007/s00024-015-1098-6.

Uddin, A., Lundberg, N., 1999. A paleo-Brahmaputra? Subsurface lithofacies analysis of Miocene deltaic sediments in the Himalayan–Bengal system, Bangladesh. Sediment. Geol. 123, 239–254. https://doi.org/10.1016/S0037-0738(98)00134-1.

Wathelet, M., Chatelain, J.-L., Cornou, C., Di Giulio, G., Guillier, B., Ohrnberger, M., Savvaidis, A., 2020. Geopsy: a User-Friendly Open-Source Tool Set for Ambient Vibration Processing. Seismol. Res. Lett. 91, 1878–1889. https://doi.org/10.1785/0220190360.

Withers, M., Aster, R., Young, C., Beiriger, J., Harris, M., Moore, S., Trujillo, J., 1998. A comparison of select trigger algorithms for automated global seismic phase and event detection. Bull. Seismol. Soc. Am. 88, 95–106. https://doi.org/10.1785/BSSA0880010095.

Wu, H., Masaki, K., Irikura, K., Sánchez-Sesma, F.J., 2017. Application of a simplified calculation for full-wave microtremor H/V spectral ratio based on the diffuse field approximation to identify underground velocity structures. Earth, Planets 69, 162. https://doi.org/10.1186/s40623-017-0746-8.